

Deep Learning Methods for Remote Heart Rate Measurement: A Review and Future Research Agenda

Chun Hong Cheng^{1,4,†} , Kwan Long Wong^{2,4,†,*}, Jing Wei Chin^{3,4}, Tsz Tai Chan^{3,4}, Richard H.Y. So^{3,4}

¹ Department of Computer Science, The Hong Kong University of Science and Technology, Clear Water Bay, Kowloon, Hong Kong

² Department of Bioengineering, The Hong Kong University of Science and Technology, Clear Water Bay, Kowloon, Hong Kong

³ Department of Industrial Engineering and Decision Analytics, The Hong Kong University of Science and Technology, Clear Water Bay, Kowloon, Hong Kong

⁴ PanopticAI, Hong Kong Science and Technology Parks, Hong Kong

* Author to whom correspondence should be addressed to.

† These authors contributed equally to this work.

Abstract: Heart rate (HR) is one of the essential vital signs used to indicate the physiological health of the human body. While traditional HR monitors usually require contact with skin, remote photoplethysmography (rPPG) enables contactless HR monitoring by capturing subtle light changes of skin through a video camera. Given the vast potential of this technology in the future of digital healthcare, remote monitoring of physiological signals has gained significant traction in the research community. In recent years, the success of deep learning (DL) methods for image and video analysis has inspired researchers to apply such techniques to various parts of the remote physiological signal extraction pipeline. In this paper, we discuss several recent advances of DL-based methods specifically for remote HR measurement, categorizing them based on model architecture and application. We further detail relevant real-world applications of remote physiological monitoring and summarize various common resources used to accelerate related research progress. Lastly, we analyze the implications of research findings and discuss research gaps to guide future explorations.

Keywords: noncontact monitoring; heart rate measurement; remote photoplethysmography; rPPG; deep learning

Citation: Cheng, C.H.; Wong, K.L.; Chin, J.W.; Chan, T.T.; So, R.H.Y. Deep Learning Methods for Remote Heart Rate Measurement: A Review and Future Research Agenda. *Sensors* **2021**, *11*, 0. <https://doi.org/>

Received:

Accepted:

Published:

Publisher's Note: MDPI stays neutral with regard to jurisdictional claims in published maps and institutional affiliations.

Copyright: © 2022 by the authors. Submitted to *Sensors* for possible open access publication under the terms and conditions of the Creative Commons Attribution (CC BY) license (<https://creativecommons.org/licenses/by/4.0/>).

1. Introduction

Human vital signs, such as heart rate (HR), body temperature (BT), respiratory rate (RR), blood oxygen saturation (SpO₂), heart rate variability (HRV), and blood pressure (BP), are common indicators used for monitoring the physiological status of the human body [1–4]. They can be used to estimate and analyze a person's physical health, detect possible diseases, and monitor recovery. In particular, closely monitoring a person's HR can enable early detection and prevention of cardiovascular problems like atherosclerosis (heart block) and arrhythmia (irregular heart rate) [5].

Photoplethysmography (PPG) is a common method for measuring HR. It utilizes a light source and photodetector to measure the volumetric changes of blood vessels under the skin [6,7]. As the light source illuminates the tissue, small variations in reflected or transmitted light intensity from blood flow are captured by the photodetector, yielding the so-called PPG signal [7]. The absorption of light follows the Beer–Lambert law, which states that the light absorbed by blood is proportional to the penetration of light into the skin and the concentration of hemoglobin in the blood [8]. During the cardiac cycle, minute variations in hemoglobin concentration cause fluctuations in the amount of light absorbed by the blood vessels, resulting in changes of skin intensity values. Pulse oximeters are commonly used for non-invasive measurement of these slight variations

34 in the skin through PPG. However, like other wearables and contact-based devices (e.g.,
 35 smartwatches), they are unsuitable for monitoring newborns or patients with fragile
 36 skin [9,10]. Furthermore, long-term monitoring may lead to discomfort and even the
 37 risk of skin infections [11]. As a result, contactless PPG methods have emerged as an
 38 attractive alternative.

39 During the last decade, rPPG methods have gained significant traction. In rPPG, a
 40 digital camera (e.g., webcam, standard RGB camera, near-infrared camera) functions as
 41 a photodetector that captures subtle color changes of the skin; ambient light typically
 42 serves as the light source [12]. Figure 1 illustrates the principle of rPPG with the dichro-
 43 matic reflection model (DRM) [13]. According to the DRM, the signals captured by the
 44 digital camera are a combination of specular reflections (surface reflections) and diffuse
 45 reflections (body reflections). Specular reflections occur at the interface of the incident
 46 light and the skin, which do not contain meaningful physiological signals. Thus, rPPG
 47 methods utilize signal processing techniques to separate the specular reflections and
 48 extract the diffuse reflections associated with the underlying signals of interest. The
 49 ability for contactless measurement can significantly reduce monitoring costs and enable
 50 applications where traditional contact sensors would be suboptimal [14]. However,
 51 while rPPG technology will undoubtedly play a pivotal role in the future of digital
 52 healthcare, the extracted signals are inherently much weaker and require meticulous
 53 processing.

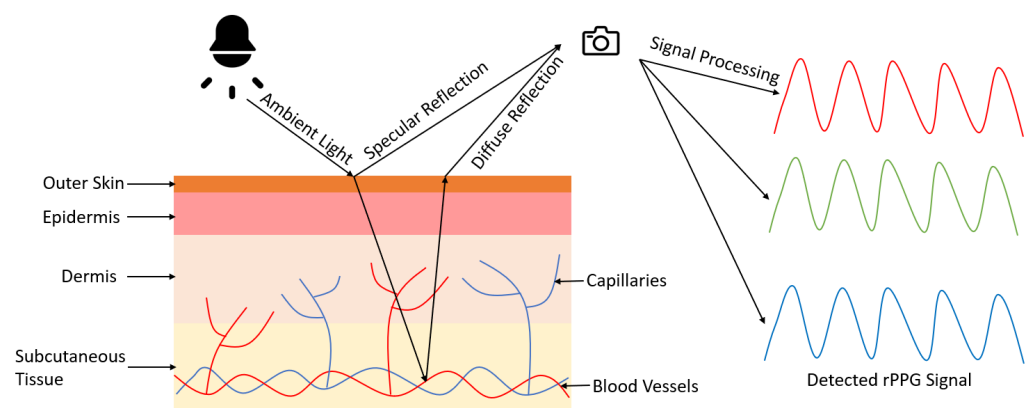


Figure 1. Principle of rPPG based on the DRM. The digital camera captures the specular and diffuse reflection from ambient light. The specular reflection contains surface information that does not relate to physiological signals, while the diffuse reflection is modulated by blood flow. The rPPG signal can be obtained from further signal processing.

54 Verkrusse et al. [15] was the initial research that used a consumer-level camera with
 55 ambient light for measurement of rPPG signals. In their work, the green channel was
 56 found to contain the most significant PPG signal. Poh et al. [16] applied a blind source
 57 separation (BSS) technique, independent component analysis (ICA), on the recorded
 58 RGB color channels from a webcam to recover HR. Lewandoska et al. [17] applied a
 59 similar method, principal component analysis (PCA), which reduced the computational
 60 complexity while achieving a similar accuracy to ICA. However, these methods are
 61 subject to motion artifacts. To improve the motion robustness of the rPPG model,
 62 a chrominance-based approach (CHROM) was proposed [18]. In this approach, the
 63 dichromatic reflection model was used to describe the light reflected from the skin as
 64 specular and diffuse reflection components [19]. De Haan and van Leest [20] defined a
 65 blood-volume pulse vector, which represents the signature of blood volume change, to
 66 identify the subtle color changes due to the pulse from motion artifacts based on RGB
 67 measurement. Later, Wang et al. [21] proposed a data-driven algorithm, spatial subspace
 68 rotation (2SR), to estimate a spatial subspace of skin pixels and evaluate its temporal
 69 rotation to measure HR. Wang et al. [13] further proposed a plane-orthogonal-to-skin

70 (POS) algorithm that defines a projection plane orthogonal to skin tone in the RGB space
 71 to extract the pulse signal. Further information about early conventional rPPG methods
 72 can be found in the following surveys [14,22,23].

73 Most conventional methods for remote HR measurement follow a similar frame-
 74 work as shown in Figure 2. Firstly, a digital camera captures a video recording of the
 75 subject. Next, a face detection algorithm, such as the Viola and Jones algorithm [24], is
 76 applied to obtain the bounding box coordinates of the subject's face. This is followed by
 77 selecting regions of interest (ROIs), such as the cheeks, to obtain an area that contains a
 78 strong signal. The pixels within the ROI(s) are used for rPPG signal extraction and HR is
 79 estimated by further post-processing, which typically involves frequency analysis and
 80 peak detection.

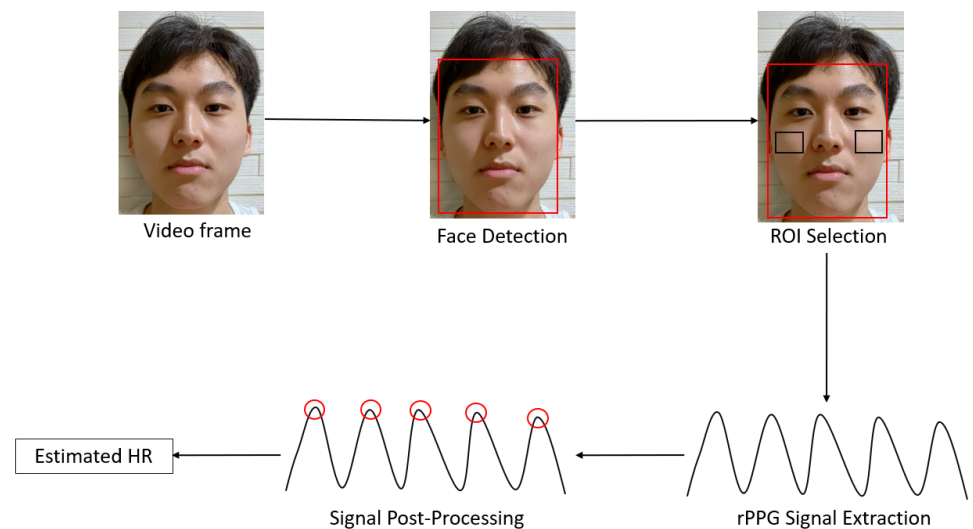


Figure 2. General framework of conventional methods for remote HR measurement. Face detection (e.g., Viola and Jones algorithm) is performed on the video frames, resulting in the red bounding box on the face. Next, the ROIs (e.g., the cheeks, black bounding boxes) are selected within the face box. The rPPG signal is extracted from the pixels within the ROI. Lastly, post-processing techniques such as frequency analysis (e.g., Fourier transform) and peak detection are applied on the extracted signal to estimate HR.

81 Like many computer vision and signal processing applications, DL methods have
 82 shown promise in mapping the complex physiological processes for remote HR mea-
 83 surement. While many review papers have discussed the conventional techniques for
 84 non-contact physiological monitoring [10,12,14,23], there is limited emphasis on DL
 85 methods, despite their popularity in the research community. The number of research
 86 papers utilizing DL methods for remote HR measurement has increased year after year
 87 and is expected to grow continuously. Our paper aims to provide researchers with
 88 an extensive review of DL approaches for remote HR measurement and an improved
 89 understanding of their benefits and drawbacks.

90 In the following sections of this paper, we categorize DL approaches for remote
 91 HR measurement as end-to-end and hybrid DL methods. We proceed to classify them
 92 based on model architecture and critically analyze their methods. We then discuss the
 93 real-world applications that benefit from this technology and introduce some common
 94 resources, including toolboxes, datasets, and open challenges for researchers in this
 95 field. Finally, we analyze the current knowledge gaps and suggest future directions for
 96 research.

97 2. End-to-End Deep Learning Methods

98 In this section, we detail the end-to-end DL approaches for remote HR measure-
 99 ment. We classify a method as end-to-end if it takes in a series of video frames as input

100 and directly outputs the HR without any intermediate steps. Since many DL methods
 101 are designed to output the rPPG signal, these are also grouped in the same category for
 102 subsequent analysis (Figure 3). As shown in Table 2, the methods are further classified
 103 based on the type of DL technique used. While end-to-end DL methods are indisputably
 104 great tools due to their straightforward model optimization process, they require enor-
 105 mous amounts of training data and are difficult to validate. More work needs to be done
 106 on the interpretation of such models for translation to clinical application [25].

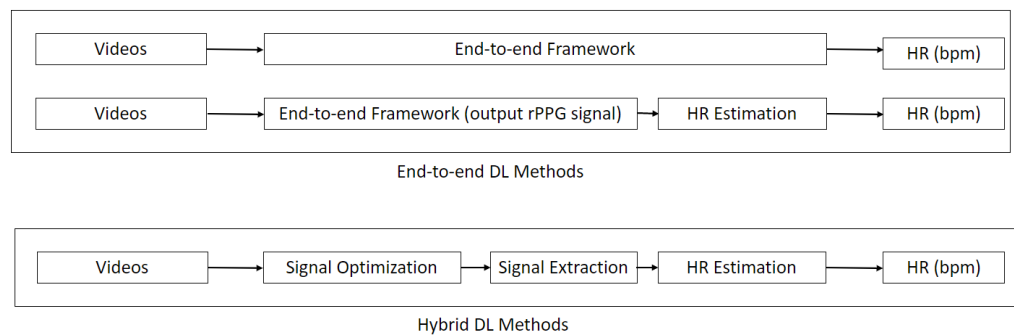


Figure 3. Schematic diagram of end-to-end DL methods and hybrid DL methods. End-to-end DL methods directly output the HR or rPPG signal with a single model while hybrid DL methods utilize DL techniques at various stages.

107 2.1. 2D Convolutional Neural Network (2D CNN)

108 Špetlík et al. [26] proposed an end-to-end HR estimation approach, where the
 109 output of the model was a single scalar value of the predicted HR. HR-CNN is a two-
 110 step CNN that contains an extractor and a HR estimator. The 2D CNN extractor was
 111 trained to maximize the signal-to-noise ratio (SNR) in order to extract the rPPG signal
 112 from a sequence of video frames. Then, the extracted rPPG signal was fed into the
 113 HR estimator to output the predicted HR value, where the training process minimized
 114 the mean absolute error (MAE) between the predicted and ground truth HR. Špetlík et
 115 al. [26] claimed that their proposed method better addressed video compression artifacts,
 116 where most conventional rPPG signal extraction methods fail. They validated it on
 117 three public datasets, and also proposed a new challenging dataset (ECG-Fitness) which
 118 contained different motions and lighting conditions.

119 DeepPhys [27] is a VGG-style 2D CNN that jointly trained a motion and appearance
 120 model (Figure 4). The motion model took the normalized difference between adjacent
 121 frames as an input motion representation; it is built on top of the dichromatic reflection
 122 model for modeling motions and color changes. The appearance model guided the
 123 motion model to learn motion representation through an attention mechanism. The
 124 network learned soft-attention masks from the original video frames and allocated
 125 higher weights to skin areas with stronger signals. This attention mechanism also
 126 enabled the visualization of the spatio-temporal distribution of physiological signals.
 127 With the motion representation and attention mechanism, Chen and McDuff [27] claimed
 128 that physiological signals under different lighting conditions can be better captured,
 129 being more robust to illumination changes and subject motion.

130 MTTs-CAN [28] is an improvement built on top of DeepPhys [27]. MTTs-CAN
 131 captured temporal information through the introduction of a temporal shift module
 132 (TSM) [29]. TSM allowed information exchange among neighboring frames and avoided
 133 expensive 3D convolution operations by shifting chunks in the tensor along the temporal
 134 axis. In addition, the input of the appearance model was a frame obtained by performing
 135 averaging adjacent multiple frames rather than the original video frame. Furthermore, it
 136 estimated HR and RR simultaneously by using a multi-task variant. Since this network

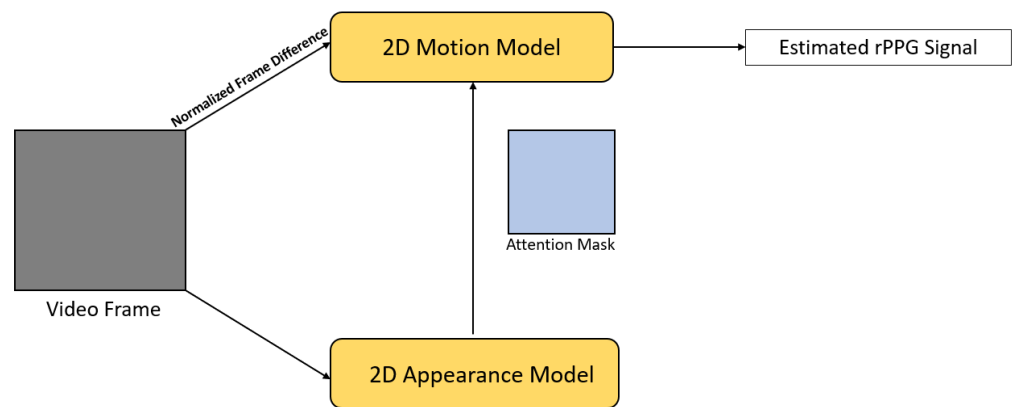


Figure 4. Architecture of DeepPhys [27].

137 was completely based on 2D CNNs, it only took 6ms per frame for on-device inference,
 138 which demonstrated its potential of being utilized in real time applications.

139 2.2. Spatio-Temporal Network — 3D Convolutional Neural Network (3D CNN)

140 As 2D CNNs only take spatial information of video frames into account, researchers
 141 have proposed different 3D CNN frameworks to also make use of the temporal infor-
 142 mation contained in the videos. These so-called spatio-temporal networks (STNs) can
 143 provide a more comprehensive representation of the spatial and temporal information
 144 of the physiological signals in the video stream.

145 3D CNN PhysNet [30] is an end-to-end STN aimed at locating the peak of every
 146 individual heartbeat (Figure 5). It is able to estimate both HR and HRV accurately,
 147 allowing more complicated applications such as emotion recognition. It took the original
 148 RGB video frames as input and directly output the final rPPG signal. In addition, it
 149 utilized the negative Pearson correlation as the loss function in order to have higher
 150 trend similarity and fewer peak location errors.

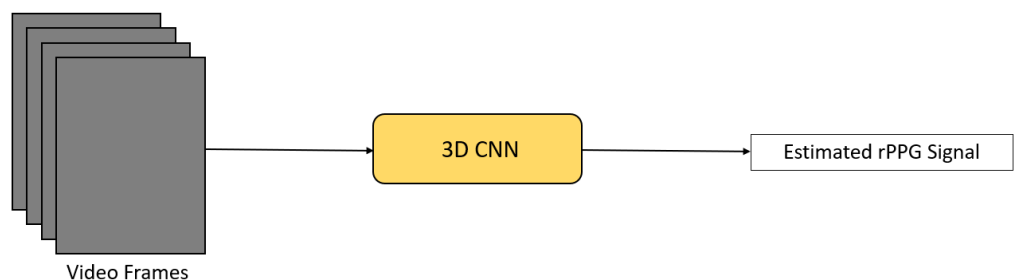


Figure 5. Architecture of 3D CNN PhysNet [30].

151 Yu et al. [31] proposed a two-stage end-to-end STN to not only estimate the rPPG
 152 signal but also to overcome the problem of highly compressed facial videos (Figure 6).
 153 Compressed facial videos were fed into a spatio-temporal video enhancement network
 154 (STVEN) to improve the quality of the videos while retaining as much information
 155 as possible. The enhanced videos were further fed into a spatio-temporal 3D CNN
 156 (rPPGNet) to extract the rPPG signal. Inside rPPGNet, an attention mechanism was
 157 applied to obtain dominant rPPG features from skin regions. rPPGNet is able to operate
 158 individually for rPPG signal extraction but can be trained jointly with STVEN to achieve
 159 better performance. Yu et al. [31] claimed that rPPGNet is able to recover better rPPG
 160 signals with curves and peak locations for accurate HR and HRV estimation.

161 Yu et al. [32] utilized neural architecture search (NAS) to automatically find the
 162 best-suited backbone 3D CNN for rPPG signal extraction (Figure 7). In their research, a
 163 special 3D convolution operation, namely temporal difference convolution (TDC), was

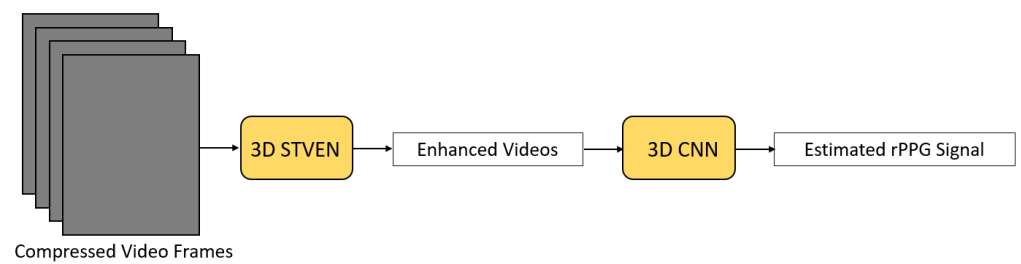


Figure 6. Architecture used in Yu et al. [31].

164 designed to help track the ROI, and improve the robustness in the presence of motion
 165 and poor illumination. Then, NAS was performed based on two gradient-based NAS
 166 methods [33,34] in order to form a backbone network for rPPG signal extraction. Two
 167 data augmentation methods were proposed as well in order to prevent data scarcity.

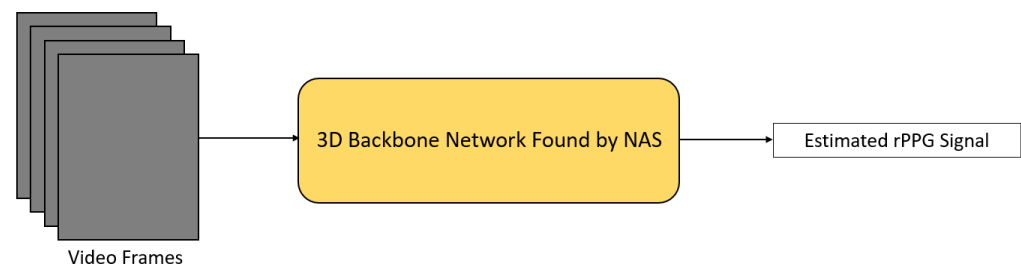


Figure 7. Architecture of AutoHR [32].

168 Hu et al. [35] designed a novel facial feature extraction method in order to avoid
 169 extracting redundant information from video segments and to enhance long-range video
 170 temporal modeling. A 3D CNN was used to extract facial features of the input video
 171 frames. Next, aggregation functions were applied to incorporate long-range spatio-
 172 temporal feature maps into short segment spatio-temporal feature maps. These feature
 173 maps were then fed into a signal extractor with several spatio-temporal convolution [36]
 174 to extract the rPPG signal. A spatio-temporal strip pooling method and an attention
 175 mechanism were further applied to the extracted rPPG signal to accommodate head
 176 movement and avoid ignoring important local information.

177 Zhang et al. [37] proposed an efficient multi-hierarchical convolutional network
 178 to perform estimation quickly, where only 15 seconds of face video was required for
 179 effectively reconstructing the rPPG signal and estimating HR. A three-layer 3D CNN
 180 was used to extract low-level facial feature maps from RGB face videos. These feature
 181 maps were passed to a spatio-temporal stack convolution module for deeper feature
 182 extraction and generation of a high-level feature map. Channel-wise feature extraction
 183 was then performed on the high-level feature map to produce a channel-wise feature
 184 map. A skin map was also generated based on low-level feature maps for emphasizing
 185 skin regions with stronger signals. Next, a weight mask was constructed by performing
 186 feature fusion on the skin map and the channel-wise feature map. Finally, the high-level
 187 feature map was multiplied by the weight mask by channels and was fed into a rPPG
 188 signal extractor.

189 ETA-rPPGNet [38] is another network aimed at dealing with the problem of extract-
 190 ing redundant video information (Figure 8). In this network, a time-domain segment
 191 subnet was designed to model the long-range temporal structure of the video. Split
 192 video segments were passed to different subspace networks of this subnet to extract
 193 facial features. Then, an attention mechanism was applied to learn important spatial
 194 features. Next, an aggregation function was used to aggregate the temporal context in
 195 order to cut down redundant video information and a feature map was obtained in each
 196 individual subspace network. These individual feature maps were concatenated and fed
 197 into the backbone network for rPPG signal extraction. Inside the backbone network, an

198 attention module was also added for eliminating different noise (e.g. head movement,
199 illumination variation). Finally, the extracted rPPG signal was further processed by a 1D
200 convolution operation to model the correlation held in the local time domain effectively.

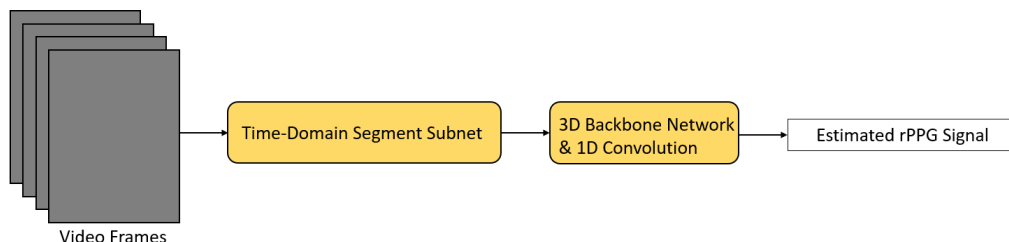


Figure 8. Architecture of ETA-rPPGNet [38].

201 **2.3. Spatio-Temporal Network — 2D Convolutional Neural Network + Recurrent Neural**
202 **Network (2D CNN + RNN)**

203 Researchers have also designed another type of spatio-temporal network, which is
204 the combination of 2D CNN for spatial information and RNN for temporal context.

205 In the same work of [30], a different version of PhysNet, which combined a 2D
206 CNN with different RNNs (LSTM, BiLSTM, ConvLSTM [39]) was proposed to compare
207 the performance of 3D CNN-based PhysNet and RNN-based PhysNet, and evaluate
208 the performance of different RNNs (Figure 9). The input and output of the network
209 remained the same as for the 3D CNN PhysNet. The input was firstly fed into a 2D CNN
210 to extract spatial features of the RGB video frames; then the RNN was used to propagate
211 these spatial features in the temporal domain. In their research, 3D CNN-based PhysNet
212 achieved a better performance than RNN-based PhysNet, and the BiLSTM variant had
213 the worst performance, indicating the backward information flow of spatial features was
214 not necessary. Table 1 shows the performance of different versions of PhysNet in terms
215 of root mean square error (RMSE) and Pearson correlation coefficient (R) [30].

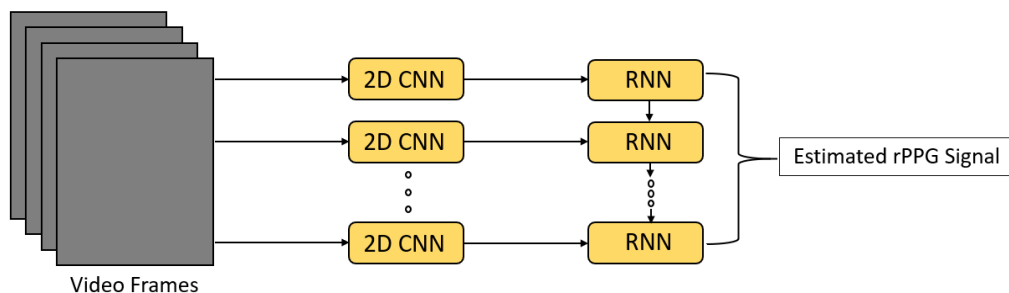


Figure 9. Architecture of RNN-based PhysNet [30].

Table 1. Performance of different versions of PhysNet [30] on the OBF [40] dataset. Root mean square error (RMSE) in beats per minute (bpm) and Pearson correlation coefficient (R) were used as the evaluation metrics.

3D CNN based	LSTM variant	BiLSTM variant	ConvLSTM variant
RMSE = 2.048, R = 0.989	RMSE = 3.139, R = 0.975	RMSE = 4.595, R = 0.945	RMSE = 2.937, R = 0.977

216 In [41], another combination of 2D CNN with a ConvLSTM network with attention
217 mechanism was proposed for rPPG signal extraction. The 2D CNN part had a similar
218 approach as DeepPhys [27], which consisted of a trunk branch and a mask branch. The
219 trunk branch was used to extract spatial features from a sequence of face images while
220 the mask branch learned and generated attention masks, and passed them to the trunk

221 branch to guide feature extraction. These spatial features were then fed into a ConvLSTM
 222 network in order to make use of the temporal correlation held in video frames for rPPG
 223 signal extraction.

Table 2. Summary of end-to-end DL methods for remote HR measurement

Ref.	Year	2D CNN	3D CNN	2D CNN + RNN	NAS	Attention
[26]	2018	✓				
[27]	2018	✓				✓
[28]	2020	✓				✓
[30]	2019		✓	✓		
[31]	2019		✓			✓
[32]	2020		✓		✓	
[35]	2021		✓			✓
[37]	2021		✓			
[38]	2021		✓			✓
[41]	2019			✓		✓

224 3. Hybrid Deep Learning Methods

225 In this section, we describe hybrid DL methods for remote HR measurement. For
 226 hybrid DL methods, DL techniques are only applied in some parts of the pipeline. We
 227 further indicate whether the methods are used for signal optimization, signal extraction
 228 or HR estimation (Figure 3).

229 3.1. Deep Learning for Signal Optimization

230 In most existing remote HR measurement pipelines, the input is the original video
 231 recorded by a digital camera. Therefore, face detection or skin segmentation is needed
 232 to ignore irrelevant background information. Moreover, some specific skin regions like
 233 the cheeks contain stronger signals and are usually selected as the ROI [42]. In this
 234 subsection, we describe these DL-based signal optimization methods to enable more
 235 effective signal extraction.

236 In [43], a 2D CNN for skin detection was created and trained on a private video
 237 database. Both skin and non-skin region samples were manually segmented and treated
 238 as positive and negative samples respectively. Conventional rPPG algorithms (ICA and
 239 PCA) were then performed on the detected skin region for evaluation. Tang et al. [43]
 240 suggested that low-cost cameras could capture rPPG signals with their method, which
 241 worked on single-channel input by choosing the RGB channel with the least noise under
 242 different conditions. This method could be combined with traditional rPPG methods in
 243 order to improve their performance. However, it utilized all the skin areas of the face for
 244 rPPG signal extraction, which may include unnecessary noise. Moreover, their method
 245 was only validated on a private dataset with yellow skin tones.

246 In [44], a single-photon avalanche diode (SPAD) camera was used to record videos.
 247 This camera was able to work well in dark environments. The recorded frame was a
 248 low-resolution grayscale image. A 2D CNN encoder-decoder model took this as input
 249 and produced a single channel image with values between zero and one, representing
 250 the probability that the particular pixel was regarded as skin. In addition, a transfer
 251 learning approach was adopted in the training process due to the lack of data for this
 252 specific skin detection problem. The model was trained on a large dataset of unlabeled
 253 face images for colorization and then further trained on a skin mask dataset. Finally, a
 254 binary skin mask was obtained by thresholding and passed for signal extraction.

255 In Deep-HR [45], a receptive field block (RFB) network was utilized to detect
 256 the ROI as an object [46]. This network was trained on a private dataset with videos
 257 recorded in realistic settings to improve overall robustness. Furthermore, a generative
 258 adversarial network (GAN)-style module was designed to enhance the detected ROI.
 259 A CNN that learned the distribution of high-quality ROIs acted as a discriminator to
 260 supervise another deep encoder-decoder network that served as a generator to regenerate
 261 the detected ROI. This high-quality detected ROI was passed for subsequent signal
 262 extraction. The architecture used for signal optimization in Deep-HR [45] is illustrated
 263 in Figure 10.

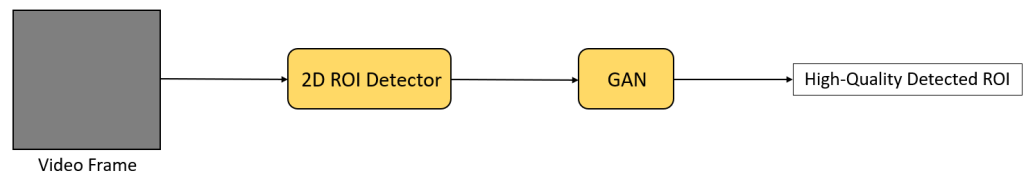


Figure 10. Architecture used in Deep-HR [45] for signal optimization.

264 3.2. Deep Learning for Signal Extraction

265 Signal extraction is the most important part in the remote HR measurement pipeline,
 266 and it is the leading focus in this research field. Its principal goal is to extract the rPPG
 267 signal from videos for HR estimation. In addition, refining the extracted rPPG signal
 268 for better HR estimation is a method to improve the estimation accuracy. Researchers
 269 have proposed many different DL methods for obtaining a high-quality rPPG signal,
 270 and we are going to categorize and describe them based on the type of neural network
 271 being used. Table 3 shows neural networks used in different DL-based signal extraction
 272 methods.

273 3.2.1. Long Short-Term Memory (LSTM)

274 In [47,48], a LSTM network was applied for signal filtering, improving the quality
 275 of the extracted rPPG signal. As the rPPG signal extracted by conventional methods may
 276 contain several noise, filtering the noise-contaminated rPPG signal is able to produce
 277 a noiseless rPPG signal for more accurate HR estimation. The LSTM network in [47]
 278 was firstly trained on a large amount of synthetic data. Then, it was further trained on
 279 real data for model fine-tuning, enhancing its generalization ability. This method is able
 280 to effectively overcome the problem of data shortage. The architecture used for signal
 281 filtering in [47] is shown in Figure 11.

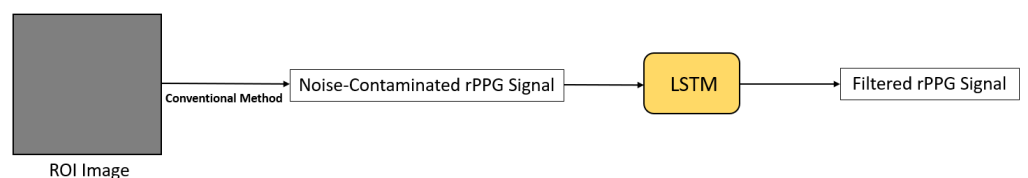


Figure 11. Architecture used in Bian et al. [47].

282 3.2.2. 2D Convolutional Neural Network (2D CNN)

283 In Deep-HR [45], a 2D CNN was learned to extract color information of the ROI
 284 pixels (Figure 12). Noise was further removed from the extracted information by using a
 285 GAN-style module. A discriminator that accesses high-quality rPPG signals was used to
 286 guide a generator to reconstruct a noiseless rPPG signal. This noise removing technique
 287 can be applied in other rPPG methods to improve the performance as well.

288 MetaPhys [49] utilized a pretrained 2D CNN, namely TS-CAN, which was another
 289 version of MTTs-CAN [28] for signal extraction. The difference between them was the
 290 use of the multi-task variant so TS-CAN could only estimate HR and RR one at a time

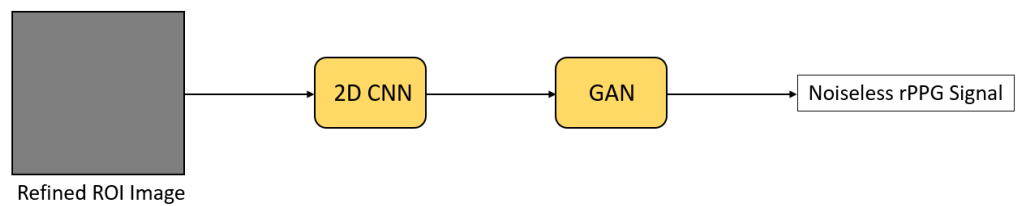


Figure 12. Architecture used in Deep-HR [45] for signal extraction.

291 while MTTS-CAN could estimate HR and RR simultaneously. Furthermore, a meta-
 292 learning approach was proposed for better generalization of the model. Model-Agnostic
 293 Meta-Learning (MAML) [50] was utilized as the personalized parameter update schema
 294 to produce a general initialization so that fast adaptation could be performed when only
 295 a few training samples were available. In addition, both supervised and unsupervised
 296 training methods were evaluated on MetaPhys. Liu et al. [49] claimed that this approach
 297 can reduce bias due to skin tone, improving the robustness of the model.

298 3.2.3. Spatio-Temporal Network — 3D Convolutional Neural Network (3D CNN)

299 In [51], a 3D CNN was designed to extract features from unprocessed video streams,
 300 followed by a multilayer perceptron to regress HR. In the paper, a data augmentation
 301 method was also proposed for generating realistic videos effectively with synthetic rPPG
 302 signals. The synthetic rPPG signal was transformed to a video by using vector repetition.
 303 Noise was also added to the synthetic videos in order to make them realistic.

304 Siamese-rPPG [52] is a framework based on a Siamese 3D CNN (Figure 13). The
 305 idea behind this framework is different facial regions may suffer from different noise and
 306 have their own appearances. However, they should reflect more or less the same rPPG
 307 characteristics. Therefore, the forehead and cheek regions with more rPPG information
 308 were firstly selected as the ROI. Next, pixels in these two ROIs were passed to the
 309 forehead branch and the cheek branch for extraction, respectively; both were 3D CNNs
 310 with the same architecture. Weight sharing mechanism was also applied to these two
 311 branches so even if either the cheek or forehead region was contaminated with noise,
 312 the framework could use the other region for signal extraction, improving the overall
 313 robustness. After that, the outputs from these two branches were fused by an addition
 314 operation, followed by two 1D convolutional operations and an average pooling, to
 315 produce the predicted rPPG signal.

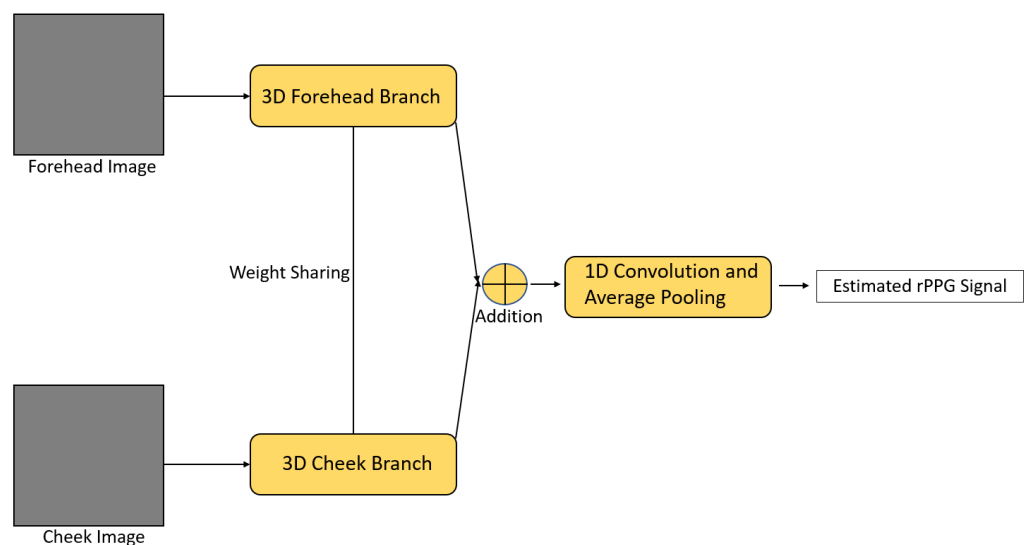


Figure 13. Architecture of Siamese-rPPG [52].

316 HeartTrack [53] utilized a 3D CNN with attention mechanism for signal extraction.
317 In this 3D spatio-temporal attention network, a hard attention mechanism was used
318 to help the network ignore unrelated background information and a soft attention
319 mechanism was used to help the model filter out covered areas. The extracted signal
320 was further fed into a 1D CNN for time series analysis. Synthetic data was also used in
321 the training process in order to address the problem of inadequate real data.

322 In [54], a multi-task framework was proposed for learning a rPPG signal extraction
323 model and augmenting data simultaneously. There were a total of 3 main networks in
324 this framework. The first one was a signal extractor that directly extracted the rPPG
325 signal from the input facial videos. The second one was a reconstruction network for
326 generating synthetic videos from real images. The third one was also a reconstruction
327 network for generating synthetic videos from real videos. They were designed to support
328 each other, and these two reconstruction networks could effectively handle the problem
329 of insufficient training data and improve the overall robustness.

330 DeeprPPG [55] is a framework that can use different skin regions as the input for
331 rPPG signal measurement, allowing customized ROI selection and wider applications.
332 It took a skin region clip from the original video as the input and a spatio-temporal
333 network was utilized to extract the rPPG signal. A spatio-temporal aggregation function
334 was also proposed for easing the side effect of regions contaminated by different noise
335 and improving the robustness of the model.

336 3.2.4. Spatio-Temporal Network — 2D Convolutional Neural Network + Recurrent 337 Neural Network (2D CNN + RNN)

338 In [56], a two-stream approach was adopted for feature extraction and rPPG signal
339 extraction. For the feature extraction stream, a 2D CNN with low-rank constraint loss
340 function was proposed to force the network to learn synchronized spatial features from
341 spatio-temporal maps, improving the robustness of face detection and ROI alignment
342 errors. For the rPPG signal extraction stream, a 2D CNN was firstly used to extract the
343 rPPG signal and then the rPPG signal was further refined by a two-layer LSTM network.
344 Lastly, the outputs from these two streams were concatenated for HR estimation.

345 In [57], a 2D CNN was used to extract spatial features and local temporal informa-
346 tion, and a LSTM network was utilized for extracting global temporal information held
347 in consecutive frames. One fully connected layer was further applied to the output of
348 the LSTM to estimate HR. This framework was able to overcome processing latency and
349 update HR in about 1 second, showing the potential of being adopted in real-time HR
350 monitoring.

351 Meta-rPPG [58] utilized a transductive meta-learner to take unlabeled data during
352 deployment for self-supervised weight adjustment, allowing fast adaptation to different
353 distribution of samples (Figure 14). In this framework, a ResNet-alike convolutional
354 encoder was firstly used to extract latent features from a stream of face images. Next,
355 these extracted features were passed to a BiLSTM network to model the temporal context,
356 followed by a multilayer perceptron (MLP) for rPPG signal estimation. A synthetic
357 gradient generator was also proposed for transductive learning. It was based on a
358 shallow Hourglass network [59] and further applied to a few-shot learning framework
359 in order to generate gradients for unlabeled data [60].

360 3.2.5. 3D Convolutional Neural Network + Recurrent Neural Network (3D CNN + 361 RNN)

362 PRNet [61] is a one-stage spatio-temporal framework for HR estimation from
363 stationary videos (Figure 15). Firstly, a 3D CNN extractor was utilized to extract spatial
364 features and capture local temporal features from the defined ROI. Next, the output
365 feature map was further fed into a LSTM extractor for extracting global temporal features.
366 Lastly, a fully connected layer was applied to estimate HR from the extracted feature
367 map. Huang et al. [61] claimed that this framework is able to predict HR with only 60

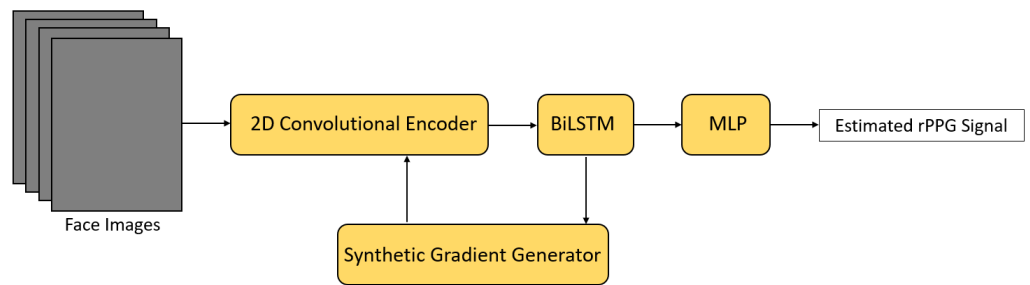


Figure 14. Architecture of Meta-rPPG [58].

368 frames of the video (2s) while other remote HR estimation methods usually need 6-30s
 369 of the video.

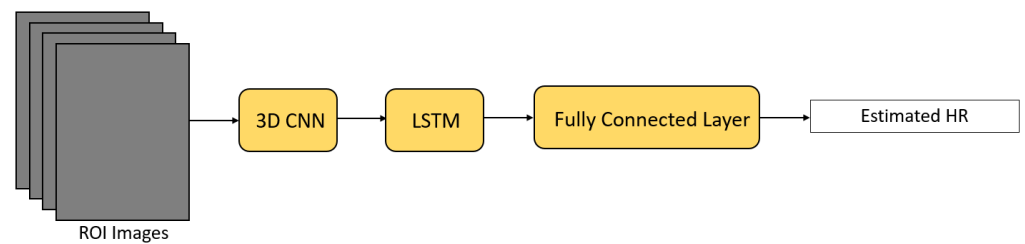


Figure 15. Architecture of PRNet [61].

370 3.2.6. Generative Adversarial Network (GAN)

371 PulseGAN [62] is a framework based on GAN to generate realistic rPPG signals
 372 (Figure 16). In the paper, a rough rPPG signal was firstly obtained by applying the
 373 CHROM algorithm on the defined ROI. Then, PulseGAN took this as input and gen-
 374 erated a high-quality, realistic rPPG signal for performing HR estimation accurately.
 375 Moreover, the structure of PulseGAN was based on the conditional GAN approach [63].
 376 The discriminator accessed the ground truth rPPG signal and guided the generator to
 377 map a rough rPPG signal extracted by CHROM to a final rPPG signal that is similar
 378 to the ground truth one. The rough rPPG signal was also set as a condition in the
 379 discriminator. Song et al. [62] mentioned that this framework can be combined with
 380 other conventional rPPG methods easily in order to improve the quality of the extracted
 381 rPPG signal, resulting in more accurate HR estimation.

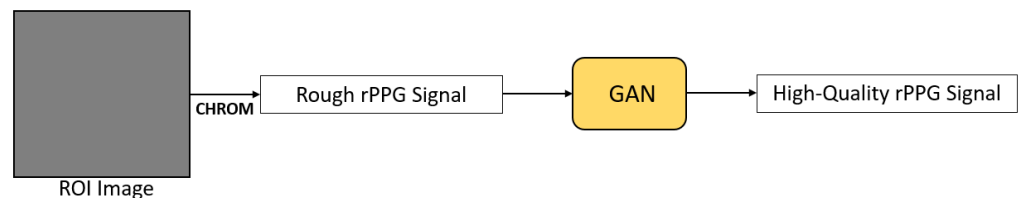


Figure 16. Architecture of PulseGAN [62].

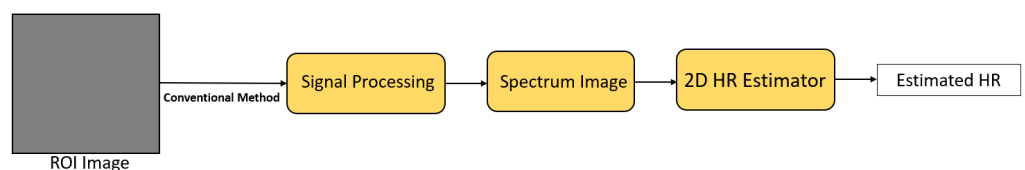
Table 3. Summary of hybrid DL methods for signal extraction in remote HR measurement pipeline

Ref.	Year	LSTM	2D CNN	3D CNN	2D CNN + RNN	3D CNN + RNN	GAN
[47]	2019	✓					
[48]	2020	✓					
[45]	2020		✓				✓
[49]	2021		✓				
[51]	2019			✓			
[52]	2020			✓			
[53]	2020			✓			
[54]	2020			✓			
[55]	2020			✓			
[56]	2019				✓		
[57]	2020				✓		
[58]	2020				✓		
[61]	2021					✓	
[62]	2021						✓

3.3. Deep Learning for Heart Rate Estimation

Traditionally, the extracted rPPG signal can be filtered with a bandpass filter followed by frequency analysis or peak detection to estimate HR. However, HR estimation can also be classified as a regression problem and solved by DL methods. Moreover, different representations of the HR signal have been proposed for DL-based HR estimation.

In [64], the rPPG signal was extracted by conventional methods (e.g., ICA, PCA, CHROM), and short-time Fourier transform and bandpass filtering were applied to the extracted rPPG signal to obtain a frequency domain representation. This representation was further combined with the time domain signal to form a spectrum image, a kind of HR signal representation. Lastly, an HR estimator based on ResNet18 [65] pretrained with the ImageNet dataset was used to estimate HR from spectrum images directly. Based on this method, HR can be estimated accurately regardless of which conventional methods were used, since the HR estimator can learn features in spectrum images and directly map them into HR. The architecture used for HR estimation in [64] is illustrated in Figure 17.

**Figure 17.** Architecture used in Yang et al. [64].

Another type of HR signal representation is the spatio-temporal map (Figure 18) used for HR estimation in [66–71]. Generally, an ROI selection step was involved in the construction of these spatio-temporal maps. Color information of the RGB channels of the ROI pixels was utilized and concatenated in temporal sequences, and placed into rows to form a spatio-temporal map. Finally, a neural network was used to estimate HR from spatio-temporal maps directly. Such kind of HR signal representation can highlight the HR signal and suppress the information that is unrelated to the HR signal. In [66,69], transfer learning was applied to pretrain the HR estimator with the ImageNet dataset to deal with insufficient data. In [67], a combination of 2D CNN and gated recurrent unit (GRU) was used for HR estimation (Figure 19). In [70], NAS was also utilized to find a

407 lightweight and optimum CNN to estimate HR from spatio-temporal maps. In [71], an
 408 attention module was added to mitigate the effect of different noise.

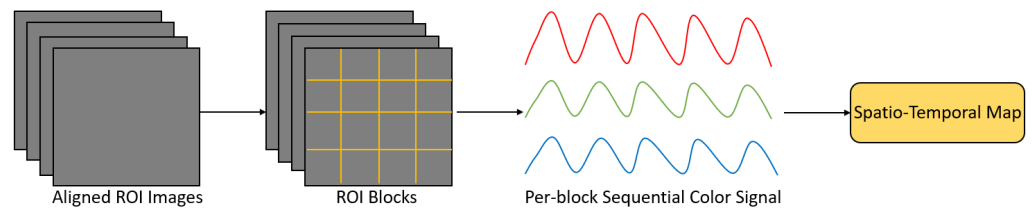


Figure 18. General procedure of constructing a spatio-temporal map. Firstly, the images are aligned and ROI selection is performed to obtain ROI images. Then, these ROI images are divided into several ROI blocks. Next, within each block, the average color value is calculated for each color channel. After that, the average color value of each channel at the same block but different frames are concatenated into temporal sequences. Finally, the temporal sequences of each block are placed into rows to form a spatio-temporal map.

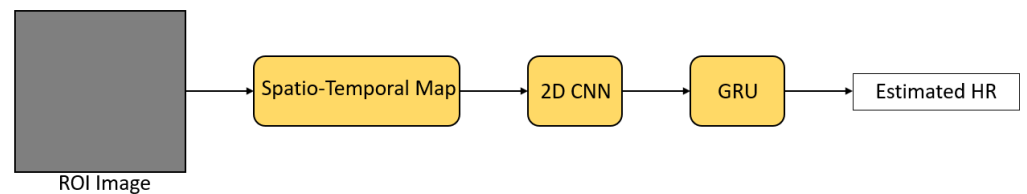


Figure 19. Architecture of RhythmNet [67].

409 HR estimation can be treated as a regression problem by using simple fully-
 410 connected layers or feedforward neural networks. In [45,56,57,61], HR was regressed
 411 by fully-connected layers from the extracted rPPG signal. The architecture used for HR
 412 estimation in [57] is shown in Figure 20. In [51,53], feedforward neural networks were
 413 also utilized to estimate HR from the extracted features.

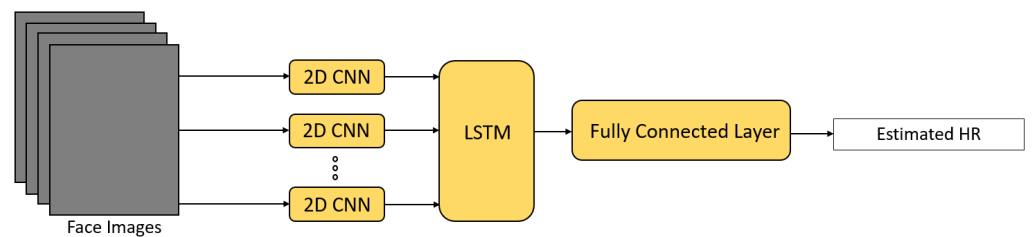


Figure 20. Architecture used in Huang et al. [57].

Table 4. Summary of all mentioned end-to-end and hybrid DL methods for remote HR measurement.

Ref.	Year	End-to-End/Hybrid	Description
[26]	2018	End-to-End	End-to-end HR estimation with an extractor and an estimator
[27]	2018	End-to-End	Normalized frame difference as motion representation, attention mechanism was used to guide the motion model, visualization of spatio-temporal distribution of physiological signals
[43]	2018	Hybrid	2D CNN network for skin detection
[64]	2018	Hybrid	Spectrum images were used for HR estimation
[66]	2018	Hybrid	Spatio-temporal maps were used for HR estimation, transfer learning approach to deal with data shortage
[30]	2019	End-to-End	Compared 3D CNN based and RNN based spatio-temporal network, can estimate HR and HRV accurately
[31]	2019	End-to-End	Enhancing video quality to deal with highly compressed videos, can estimate HR and HRV accurately
[41]	2019	End-to-End	Attention mechanism was used to guide the trunk branch for signal extraction
[47]	2019	Hybrid	LSTM network for signal filtering, transfer learning approach to deal with data shortage
[51]	2019	Hybrid	3D CNN for signal extraction, data augmentation method for generating videos with synthetic rPPG signals, multilayer perceptron for HR estimation
[56]	2019	Hybrid	2D CNN based two-stream approach for signal extraction, and LSTM network for signal refining
[71]	2019	Hybrid	Spatio-temporal maps were used for HR estimation, attention mechanism was applied to remove noise
[28]	2020	End-to-End	Temporal shift module to model temporal information, attention mechanism was applied to guide the motion model, able to estimate HR and RR simultaneously by one network
[32]	2020	End-to-End	Used NAS to find a well-suited network for HR estimation
[44]	2020	Hybrid	2D CNN encoder-decoder model for skin detection, transfer learning approach to deal with data shortage
[45]	2020	Hybrid	Two GAN-style modules to enhance the detected ROI and remove noise, 2D CNN for signal extraction
[48]	2020	Hybrid	LSTM network for signal filtering
[52]	2020	Hybrid	Siamese 3D CNN for signal extraction
[53]	2020	Hybrid	3D CNN with attention mechanism for signal extraction, feedforward neural network for HR estimation
[55]	2020	Hybrid	3D CNN that can take different skin regions for signal extraction
[57]	2020	Hybrid	2D CNN + LSTM spatio-temporal network for signal extraction
[58]	2020	Hybrid	2D CNN + BiLSTM spatio-temporal network for signal extraction, meta-learning approach for fast adaptation
[67]	2020	Hybrid	Spatio-temporal maps were used for HR estimation
[68]	2020	Hybrid	Spatio-temporal maps were used for HR estimation
[69]	2020	Hybrid	Spatio-temporal maps were used for HR estimation, transfer learning approach to deal with data shortage
[35]	2021	End-to-End	Avoid extracting redundant information from video segments, attention mechanism was applied to deal with different noise
[37]	2021	End-to-End	An efficient framework for performing HR estimation quickly
[38]	2021	End-to-End	Dealt with the problem of extracting redundant video information, attention mechanism was applied to learn important features and eliminate noise
[49]	2021	Hybrid	TS-CAN from another paper was utilized for signal extraction, meta-learning approach for fast adaptation
[54]	2021	Hybrid	Multi-task framework for simultaneous signal extraction and data augmentation
[61]	2021	Hybrid	3D CNN + LSTM spatio-temporal network for signal extraction
[62]	2021	Hybrid	GAN for generating high-quality rPPG signal from rough rPPG signal
[70]	2021	Hybrid	Spatio-temporal maps were used for HR estimation, NAS was used to find a CNN for mapping spatio-temporal maps into HR

414 4. Applications

415 With further research and inevitable technological advances, remote health moni-
416 toring technology will undoubtedly play a vital role in many aspects. The utilization of
417 contactless HR monitoring introduces benefits that existing contact-based PPG meth-
418 ods lack. In this section, we describe a few potential applications enabled by remote
419 monitoring of physiological signals.

420 4.1. Affective Computing

421 Since rPPG technology can be integrated with consumer-level cameras, it has
422 great potential for affective computing and human–computer interaction applications.
423 Researchers have demonstrated the feasibility of rPPG-based methods for interpreting
424 human affects such as cognitive stress estimation [72,73], emotion recognition [30,74],
425 engagement detection [75] and pain recognition [76–78]. These studies illustrate the
426 capability of using rPPG technology beyond the medical domain.

427 4.2. Pandemic Control

428 With the current COVID-19 outbreak, the value of contactless HR monitoring has
429 become very clear, particularly for screening the public. It has been reported that tem-
430 perature screening alone is an insufficient indication for coronavirus infection [79,80].
431 Therefore, the accuracy of screening based on temperature decreases because asymp-
432 tomatic but infected patients have a temperature within the normal range [81,82]. Given
433 this inadequacy, using HR as a criterion for COVID-19 screening was investigated.
434 In [83,84], it was shown that tachycardia (high HR) is also a symptom of COVID-19.
435 Moreover, the relationship between atrial fibrillation (AF) and COVID-19 was observed
436 in several studies [85–87], suggesting rPPG-based AF detection would be useful for
437 discovering potential COVID-19 patients [88]. Meanwhile, during and since the pan-
438 demic, the use of wearable smart devices for measuring vital signs such as HR, BP, and
439 SpO₂, have become widespread [89,90]. Such contact-based methods can be replaced by
440 rPPG technology to provide convenience to users with precise screening and detection,
441 resulting in more efficient and effective pandemic control.

442 4.3. Deepfake Detection

443 Recently, deepfake, a technology to produce high-synthetic videos with DL imple-
444 mentations, has attracted researchers' attention. Unfortunately, if not tragically, this
445 technology has been used to generate fake news and hoax videos, posing threats to the
446 society. For example, a high-quality video of the 44th President of the United States
447 Barack Obama has been synthesized by using a DL approach [91], which shows him
448 apparently making a speech that he never actually made. These fake videos are of
449 such high quality such that they are indistinguishable to humans and even complicated
450 computer vision algorithms [92–94]. As a result, deepfake detection methods need to
451 be developed to encounter such problems. Currently, there have been few attempts
452 in capturing abnormalities in biological signals like HR as a means to detect deepfake
453 videos [95,96].

454 4.4. Telehealth

455 Within the last few years, telehealth has become more popular all over the world,
456 with more than half of the health care organizations in the U.S making use of the ser-
457 vice. [97]. The integration of telehealth with rPPG technology provides various benefits
458 to the users and society. For instance, users will experience a better daily workflow
459 since the time required to travel to healthcare institutions for health-checkups and for
460 doctor consultations will be reduced. Furthermore, the application of telehealth software
461 intertwined with rPPG technology allows the user to measure their physiological signs
462 and detect early symptoms of different health problems (e.g. atrial fibrillation) from
463 any location by using a consumer-level device [88,98,99]. Deploying rPPG technology

464 promotes social distancing and safety for those healthcare workers at the front lines. Fur-
465 thermore, remote health monitoring can reduce the workload of hospitals and minimize
466 the chance of spreading diseases since it encourages less physical contact with patients
467 and fewer human resources are needed [100], which is especially vital during the midst
468 of a pandemic.

469 4.5. Face Anti-spoofing

470 Nowadays, using biometric information of individuals for authentication is very
471 common. One of the most common forms is facial recognition, which is based on the
472 analysis of unique features of a person's face [101]. However, biometric presentation
473 attacks can exist alongside the face authentication process. For example, attackers
474 can source photos (photo attacks) or videos (replay attacks) of the person from social
475 networking sites easily and present them to the authentication system [102]. Remote HR
476 measurement technology can be incorporated to enhance the authentication system [103].
477 In [104–108], rPPG-based face presentation attack detection approaches were developed,
478 suggesting the potential of rPPG technology in the security industry.

479 4.6. Driving Condition Monitoring

480 In order to reduce the number of traffic accidents, rPPG technology can be adopted
481 to monitor drivers and track a driver's physiological status. Most road accidents are
482 caused by human factors including fatigue, drowsiness, and illness. Factors such as
483 disparity in oxygen levels, HR, and RR may lead to non-specific health problems, which
484 interfere with or degrade decision-making capabilities. This monitoring allows abnormal
485 vital signs to be detected early, with alerts shown immediately so that drivers can adjust
486 their behavior accordingly, avoiding accidents. There have been several attempts for
487 monitoring drivers' physiological conditions using rPPG methods [109–118]. In [112,
488 116,118], a near-infrared camera was used instead of an RGB camera for monitoring.
489 In [113,115], neural networks were applied for physiological signal estimation.

490 4.7. Searching for Survivors during Natural Disasters

491 During natural disasters like earthquakes and fires, searching for survivors becomes
492 a vital but extremely challenging task. Rescue teams must operate in extremely haz-
493 ardous conditions like collapsed buildings. rPPG technology can be a potential way to
494 reduce risk for search and rescue teams, and improve their efficiency. In [119–121], an
495 unmanned aerial vehicle (UAV) or a drone was used to capture videos, representing a
496 more convenient, safe, and effective way to look for survivors. In [122], research using a
497 drone for multiple subject detection over a long-distance was conducted. This illustrates
498 the potential of using controllable devices equipped with a camera combined with rPPG
499 technology for searching for survivors.

500 4.8. Neonatal Monitoring

501 As neonates or infants have very sensitive and fragile skin, using contact-based
502 methods to measure their health conditions is inappropriate. rPPG methods are one
503 of the suitable candidates for long-term physiological status monitoring of newborns
504 in neonatal intensive care units (NICU). Several studies have trialed rPPG methods
505 for such monitoring [123–133]. In [132], DL-based segmentation was utilized to reduce
506 computational time, which brought it one step closer to real-time applications. In [133],
507 DL-based ROI detection was applied to handle pose variations and illumination changes,
508 further improving the estimation accuracy. These examples indicate the promise of using
509 rPPG technology for neonatal monitoring.

510 4.9. Fitness Tracking

511 During fitness training, having health monitors to keep track of the current physio-
512 logical condition is an excellent way to prevent over-exercising and help to adjust the

513 fitness process to an individual's real-time needs and condition. Contact-based methods
514 such as smartwatches or digital bracelets for such monitoring can cause discomfort or
515 pain during heavy exercise. rPPG technology can be utilized to provide simple remote
516 fitness tracking. In [134–138], rPPG methods in fitness training settings were studied.
517 In [134,137,138], motion artifact during exercise was the major focus. In [135,136], a feed-
518 back control system was implemented as well for adjusting the speed of the treadmill
519 automatically.

520 5. Resources

521 As remote physiological monitoring is an emerging field in computer vision and
522 biomedical engineering, there are resources available for researchers to accelerate progress
523 and ease the transition of newcomers. In this section, we detail some of the open-source
524 toolboxes to help to implement related algorithms and most of the datasets that are
525 commonly used for model training and benchmarking. Furthermore, open challenges in
526 rPPG are also described to encourage various researchers to contribute to the field.

527 5.1. Toolboxes

528 iPhys [139] is an open-source toolbox written in MATLAB. It contains commonly
529 used implementations in rPPG pipelines like face detection, ROI definition, and skin
530 segmentation. It also includes four conventional rPPG methods for baseline compar-
531 ison. Other plotting and signal quality calculation functions are provided as well for
532 performance evaluation.

533 In [140], the whole rPPG pipeline based on ICA and some utilities are written in
534 MATLAB. Beginners can quickly run or even modify the provided script to evaluate the
535 performance of the particular rPPG method.

536 The Python tool for Virtual Heart Rate (pyVHR) [141] is a recently developed
537 Python package for heart rate estimation based on rPPG methods. In this package, 8
538 conventional rPPG methods are implemented and evaluated based on 5 datasets. Other
539 frequently used pre-processing and post-processing techniques are provided as well.
540 Practitioners can extend the framework to evaluate their own algorithms on these 5
541 datasets.

542 5.2. Datasets

543 Performance evaluation is important for researchers to test whether their proposed
544 methods are good enough when compared with other methods and able to solve existing
545 challenges. For supervised methods, datasets are also crucial for proper training and
546 achieving state-of-the-art performance. In this subsection, we detail most of the datasets
547 that are commonly used for benchmarking and model training.

548 AFRL [142] is a dataset proposed by the United States Air Force Research Laboratory.
549 It was aimed to evaluate the effect of head motion artifacts. During data acquisition, a
550 multi-imager semicircular array (a total of 9 synchronized, visible spectrum imagers)
551 centered on the imaged participant in a controlled light environment was used to record
552 the participant's head motions during specific tasks. At the same time, electrocardiogram
553 (ECG) and fingertip reflectance PPG were recorded as ground truth signals. The imaged
554 participant was told to perform specific tasks, which included staying still, sweeping
555 around the imagers with a pre-defined angle per second, and randomly re-orienting the
556 head position to an imager. The background of the environment consisted of either a
557 solid black fabric or a patterned, colored fabric.

558 COHFACE [143] is a publicly available dataset proposed by the Idiap Research
559 Institute. The purpose of proposing this dataset was to allow researchers to evaluate
560 their developed rPPG algorithms on a publicly available dataset so that comparisons
561 between different algorithms could be conducted in a standard and principled manner.
562 In this dataset, a conventional webcam was used to capture the full face of the participant
563 in two different illumination settings (studio lighting and natural lighting) to evaluate

564 the effect of illumination variation. Skin reflectance PPG and respiratory signal were
565 recorded as ground truth signals. The only disadvantage of this dataset was the heavy
566 compression, so noise artifact was added unavoidably.

567 MAHNOB-HCI [144] is a multimodal dataset that was originally recorded for
568 emotion recognition and implicit tagging research. However, as ground truth signals like
569 ECG and respiration amplitude were recorded, it was also suitable for rPPG algorithm
570 evaluation. Moreover, six cameras were used to capture different views (frontal view,
571 profile view, wide angle, close ups) of the participant, which made this dataset useful for
572 evaluating the algorithm when pose angle varied.

573 MMSE-HR [145] is another multimodal dataset proposed for facial expression
574 analysis. Some vital signs like BP, RR, and HR were also recorded, making this dataset
575 appropriate for testing rPPG algorithms. Furthermore, subjects from different races
576 (Black, White, Asian, Hispanic/Latino) participated in the data acquisition so researchers
577 were able to evaluate their proposed methods against different skin tones.

578 OBF [40] is a large dataset made by the University of Oulu in Finland specifically for
579 remote physiological signal measurement. Aside from healthy subjects in this dataset,
580 patients with atrial fibrillation (AF) also participated in data collection in order to validate
581 rPPG methods for clinical applications like diagnosing cardiac diseases. In addition,
582 there were two different recording states, one for healthy participants and one for AF
583 patients. Healthy participants were recorded in a resting state and a post-exercise state (5
584 minutes exercise). AF patients were recorded before and after cardioversion treatment.

585 PURE [146] is a dataset proposed for examining head motion artifacts in rPPG
586 methods in more detail. During data acquisition, participants were told to perform six
587 different tasks (holding steady, talking, slow translation, fast translation, small rotation,
588 medium rotation) in order to introduce different kinds of head motion. Naturally
589 changing illumination (daylight with clouds through a large window) was used for
590 recording as well.

591 UBFC-RPPG [147] is another dataset proposed mainly for rPPG algorithm evalu-
592 ation. The data recording was conducted indoors with indoor illumination and slight
593 changes in sunlight. One special aspect of the recording is that participants were told
594 to play a time-sensitive mathematical game. Its purpose was to augment the HR of
595 participants and hence simulate a real-life human-computer interaction scenario for
596 evaluation.

597 VIPL-HR [148] is a large-scale multimodal dataset created for remote pulse esti-
598 mation research. In this dataset, various face variations due to head motion (stable,
599 large motion, talking), illumination changes (lab, dark, bright) and acquisition diversity
600 (smartphone, webcam, RGB-D camera) were introduced in order to test the overall
601 robustness of the proposed algorithm. The dataset was compressed with different codecs
602 (MJPG, FMP4, DIVX, PIM1, X264) in order to retain the completeness of the signals as
603 much as possible while being convenient for public access at the same time.

604 A summary of the mentioned datasets is provided in Table 5. Moreover, Table 6
605 illustrates the performance of all mentioned DL methods on these common datasets.
606 The evaluation metrics in Table 6 include root mean square error (RMSE) in bpm, mean
607 absolute error (MAE) in bpm, Pearson correlation coefficient (R), and signal-to-noise
608 ratio (SNR) in decibels (dB).

609 5.3. Open Challenge on Remote Physiological Signal Sensing

610 Creating an open challenge on a specific machine learning task is a common way in
611 the field of machine learning to encourage people to participate and solve a particular
612 problem using DL methods. One of the most famous open challenges is the ImageNet
613 Large Scale Visual Recognition Challenge (ILSVRC) [149]. This challenge has been
614 running annually for 8 years (2010-2017), and its focuses are object recognition, object
615 detection, and image classification. Many DL methods have been proposed for this task,
616 and this competition has definitely boosted research interest in this field, allowing rapid

617 development in DL-based computer vision. An open challenge on remote physiological
 618 signal sensing was also organized in 2020, namely Remote Physiological Signal Sensing
 619 (RePSS 2020) [150]. In this challenge, the focus was measuring the average HR from color
 620 facial videos. The VIPL-HR-V2 dataset, which is the second version of VIPL-HR [148]
 621 and the OBF dataset [40] were used for model training and testing. The RePSS 2021
 622 is also currently running, and its focus was changed to measure inter-beat-interval
 623 (IBI) curve and RR. This open challenge can have the same optimistic effect as ILSVRC,
 624 encouraging people to participate and engage in this research field.

Table 5. Summary of common datasets for remote physiological monitoring.

Dataset	Subjects	Description
AFRL [142]	25	9 RGB cameras with 120 fps, resolution is 658x492, ECG, PPG, RR are recorded
COHFACE [143]	40	1 RGB webcam with 20fps, resolution is 640x480, BVP, RR are recorded
MAHNOB-HCI [144]	27	1 RGB camera with 60 fps, 5 monochrome cameras with 60 fps, both resolution are 780x580, ECG, RR are recorded
MMSE-HR [145]	140	1 3D stereo imaging sensor with 25fps, 1 2D video sensor with 25fps, 1 thermal sensor with 25fps, RGB sensor resolution is 1040x1392, thermal sensor resolution is 640x480, HR, RR, BP are recorded
OBF [40]	106 (6 with atrial fibrillation)	1 RGB camera with 60fps, 1 NIR camera with 30 fps, RGB camera resolution is 1920x1080, NIR camera resolution is 640x480, ECG, BVP, RR are recorded
PURE [146]	10	1 RGB camera with 30 fps, resolution is 640x480, HR, SpO ₂ , PPG are recorded
UBFC-RPPG [147]	42	1 RGB webcam with 30 fps, resolution is 640x480, HR, PPG are recorded
VIPL-HR [148]	107	1 RGB webcam with 25 fps, 1 RGB-D camera with 30 fps, 1 smartphone camera with 30 fps, RGB webcam resolution is 960x720, RGB-D NIR camera resolution is 640x480, RGB-D RGB camera resolution is 1920x1080, smartphone camera resolution is 1920x1080, HR, SpO ₂ , BVP are recorded

Table 6. Performance of all mentioned end-to-end and hybrid DL methods for HR measurement on commonly used datasets listed in Table 5. [43], [44] and [57] are not included here as they are evaluated on their own private datasets.

Methods	AFRL	COHFACE	MAHNOB-HCI	MMSE-HR	OBF	PURE	UBFC-RPPG	VIPL-HR
[26]	X	RMSE = 10.78 MAE = 8.10 R = 0.29	RMSE = 9.24 MAE = 7.25 R = 0.51	X	X	RMSE = 2.37 MAE = 1.84 R = 0.98	X	X
[27]	MAE = 2.45 SNR = 4.65	X	MAE = 4.57 SNR = -8.98	X	X	X	X	X
[64]	X	X	RMSE = 4.26 R = 0.81	X	X	X	X	X
[66]	X	X	RMSE = 4.49	RMSE = 6.83	X	X	X	X
[30]	X	X	RMSE = 7.88 MAE = 5.96 R = 0.76	X	RMSE = 1.812 R = 0.992	X	X	X
[31]	X	X	RMSE = 5.93 MAE = 4.03 R = 0.88	X	RMSE = 1.8 R = 0.992	X	X	X
[41]	X	RMSE = 11.88 MAE = 7.31 R = 0.36 SNR = -1.93	X	X	X	RMSE = 1.58 MAE = 0.88 R = 0.99 SNR = 9.18	X X X X	X X X X
[47]	X	X	X	RMSE = 3.187 MAE = 4.35 R = 0.8254	X	X	X	X
[51]	X	X	X	X	X	X	RMSE = 8.64 MAE = 5.45	X X
[56]	X	RMSE = 9.96 MAE = 8.09 R = 0.40	X	X	X	X	X	X
[71]	X	X	X	RMSE = 10.10 R = 0.64	X	X	X	RMSE = 7.99 MAE = 5.40 R = 0.66
[28]	RMSE = 3.72 MAE = 1.45 R = 0.94 SNR = 8.64	X	X	RMSE = 5.66 MAE = 3.00 R = 0.92 SNR = 2.37	X	X	X	X
[32]	X	X	RMSE = 5.10 MAE = 3.78 R = 0.86	RMSE = 5.87 R = 0.89	X	X	X	RMSE = 8.68 MAE = 5.68 R = 0.72
[45]	X	X	RMSE = 3.41 R = 0.92	X	X	X	X	X
[48]	X	X	X	MAE = 1.31 SNR = 9.44	X X	X X	X X	X X
[52]	X	RMSE = 1.29 MAE = 0.70 R = 0.73	X	X	X	RMSE = 1.56 MAE = 0.51 R = 0.83	RMSE = 0.97 MAE = 0.48	X
[53]	X	X	X	X	X	X	RMSE = 3.368 MAE = 2.412 R = 0.983	X
[55]	X	RMSE = 7.06 MAE = 3.07 R = 0.86	RMSE = 6.26 MAE = 4.81 R = 0.79	X	X	RMSE = 0.43 MAE = 0.28 R = 0.999	X	X
[58]	X	X	RMSE = 3.68 MAE = 3.01 R = 0.85	X	X	X	RMSE = 7.42 MAE = 5.97 R = 0.53	X
[67]	X	X	RMSE = 3.99 R = 0.87	RMSE = 5.49 R = 0.84	X	X	X	RMSE = 8.14 MAE = 5.30 R = 0.76
[68]	X	X	X	RMSE = 6.04 R = 0.84	RMSE = 1.26 R = 0.996	X	X	RMSE = 7.97 MAE = 5.02 R = 0.796
[69]	X	X	RMSE = 3.23 MAE = 1.53 R = 0.97	X	X	X	X	X
[35]	X	RMSE = 7.52 MAE = 5.19 R = 0.68	X	X	X	RMSE = 1.21 MAE = 0.74 R = 1.00	X	X
[37]	X	RMSE = 9.50 MAE = 5.57 R = 0.75	X	X	X	X	RMSE = 3.82 MAE = 2.15 R = 0.97	X
[38]	X	RMSE = 6.65 MAE = 4.67 R = 0.77	X	RMSE = 5.84 R = 0.85	X	RMSE = 0.77 MAE = 0.34 R = 0.99	RMSE = 3.97 MAE = 1.46 R = 0.93	X
[49]	X	X	X	RMSE = 3.12 MAE = 1.87 R = 0.89	X	X	RMSE = 3.12 MAE = 2.46 R = 0.96	X
[54]	X	RMSE = 1.65 MAE = 0.68 R = 0.72	X	X	X	RMSE = 1.07 MAE = 0.40 R = 0.92	RMSE = 2.09 MAE = 0.47	X
[61]	X	X	RMSE = 6.42 MAE = 5.01	X	X	X	RMSE = 7.24 MAE = 5.29	X
[62]	X	X	RMSE = 6.53 MAE = 4.15 R = 0.71	X	X	RMSE = 4.29 MAE = 2.28 R = 0.99	RMSE = 2.10 MAE = 1.19 R = 0.98	X
[70]	X	X	X	X	X	RMSE = 2.02 MAE = 1.65 R = 0.99	X	RMSE = 8.01 MAE = 5.12 R = 0.79

6. Research Gaps

During the last few decades, many methods for ascertaining remote HR measurements have been proposed. This has attracted much attention, and increasing numbers of researchers are engaged in this exciting area. In this section, we discuss some of the research gaps in order to suggest some possible future directions in this field.

6.1. Influencing Factors

The performance of remote HR measurement based on rPPG is influenced by many factors such as illumination changes, motion artifacts, skin-tone variations, and video compression [12,14,22,23,151]. There are several methods proposed for handling these challenges. For example, the utilization of different HR signal representations like spectrum images [64] and spatio-temporal maps [66–71], and also the use of attention mechanism [27,28,31,35,38,41,49,53,71] can deal with illumination variations and motion noise. STVEN [31] was designed to improve the robustness of HR measurement under video compression. Meta-learning approaches with fast adaptation to uncommon samples [49,58] are suitable to deal with skin-tone variations. Additional work is needed to better understand and quantify the effects these influencing factors have on remote physiological measurement. More importantly, new methods should provide insight into how these challenges are handled from a technical and biophysical perspective, rather than just evaluating their performance on a dataset that contains the influencing factors.

6.2. Measuring Other Vital Signs

Undoubtedly, HR is a very important physiological indicator to indicate the current health condition of a person. Researchers in this field are mainly interested in estimating HR, followed by RR. However, other vital signs are also important [152,153]. For example, BP is useful in detecting some cardiovascular diseases like hypertension while SpO₂ can reflect the health of the cardiorespiratory system by showing if a person has an adequate supply of oxygen. At the same time, these vital signs are associated to COVID 19 and they are useful for COVID 19 diagnosing as well [154,155]. There are relatively fewer studies that attempt to estimate BP [156–158] and SpO₂ [159–161] remotely when compared HR and RR. There are still many research opportunities in other vital signs.

6.3. Datasets

Datasets are increasingly important for evaluating new proposed methods whether demonstrating success in addressing specific problems or increasing the effectiveness of previously proposed methods. For DL methods, datasets are even more important as they are used for training in supervised methods as well. The performance of the supervised methods are greatly affected by the training datasets. Currently, most of the existing publicly available datasets focus on two major challenges in rPPG methods only, that is, motion artifacts and illumination variations [12,23]. Other challenges like skin-tone variations [22,162,163], multiple persons detection [14,122] and long distance estimations [14,164] need to be overcome as well if the methods are to be, ultimately, robust and highly applicable in the real-world, replacing all contact-based methods. Moreover, the subjects in these datasets are mainly adult participants. Datasets with newborns as participants are also desirable for evaluating rPPG methods. As a result, more comprehensive, high diversity and high quality datasets are needed to fully evaluate the robustness of any new proposed method and allow comprehensive training in supervised methods. Such datasets are extremely beneficial to the research community.

6.4. Performance on Different Heart Rate Ranges

According to performance results of RePSS 2020 [150], the top 3 teams were able to achieve a significantly better performance on the middle HR level, where HR ranges from 77 to 90 bpm, followed by the low HR level (less than 70 bpm). Performance at the high

675 HR level (more than 90 bpm) was the worst. This is a challenge that absolutely needs to be
676 addressed in order to be accurate enough to be applied in real-world applications because
677 these significantly lower or higher HRs are showing specific health problems. Moreover,
678 this result indicates that using common metrics like mean absolute error (MAE), root
679 mean square error (RMSE), signal-to-noise ratio (SNR) and Pearson correlation coefficient
680 (R) to evaluate rPPG methods may not be effective enough. Evaluation on a wider range
681 of HR levels is required in order to comprehensively test the robustness of the proposed
682 method.

683 6.5. Understanding of Deep Learning-Based Methods

684 The advantage of using CNN in rPPG technology is that a good result can be
685 obtained without very deep understanding or analysis of the specific problem; the
686 disadvantage is that this DL method is a black box, which means we do not have a
687 full understanding of why such a result is obtained. The lack of understanding of how
688 CNN-based methods work on rPPG technology may be a barrier to further development
689 of this technology and evaluation of these DL methods. [25] is a work that focused on
690 the understanding of CNN-based rPPG methods rather than proposing a new model
691 with state-of-the-art performance. Several experiments were performed to explore the
692 CNN-based rPPG signal extraction and improve the understanding of this approach.
693 In the paper, some important observations have been made. For example, it showed
694 that the CNN for rPPG signal extraction is actually learning information related to the
695 PPG signal but not the motion-induced intensity changes [27]. In addition, the CNN
696 training is affected by the physiological delay between the video data and the reference
697 finger oximeter. Researchers should direct their attention to more studies that focus on
698 the understanding of DL-based rPPG methods in order to gain valuable insights and
699 further improve the performance of these DL approaches.

700 7. Conclusion

701 In recent years, many methods for remote HR measurement have been proposed.
702 Due to rapid development in the area of machine learning, DL methods have shown
703 significant promise in this field. In this paper, we have provided a comprehensive
704 review on most of the existing recent DL-based methods for remote HR estimation. We
705 have further categorized these methods into end-to-end and hybrid DL methods, and
706 grouped them based on the type of neural network being used. We then described some
707 potential applications that can be achieved by using rPPG technology. Next, some rPPG
708 resources like toolboxes, datasets and open challenges have been detailed in order to
709 help accelerate research. Lastly, we have discussed some of the current research gaps in
710 this field to shed some light on future areas and directions in this exciting field.

711 As remote physiological measurement establishes itself as an emerging research
712 field, we suggest more work should focus on addressing different influencing factors
713 and estimating other vital signs, which will assist in bridging the gap for real-world
714 applications. Furthermore, high-quality and diverse datasets are crucial for proper
715 benchmarking and analysis of different methods and the future development of more
716 complex DL models and architectures. Last but not least, the understanding of different
717 DL-based approaches is critical, especially when integrating these networks for high-
718 stakes applications like healthcare diagnostics.

719 **Author Contributions:** C.H.C and K.L.W performed the literature review and prepared the draft
720 manuscript. J.W.C, T.T.C and R.H.Y.S reviewed and edited the manuscript. All authors have read
721 and agreed to the published version of the manuscript.

722 **Funding:** This research is partially funded by the Technology Start-up Support Scheme for
723 Universities.

724 **Institutional Review Board Statement:** Not applicable.

725 **Informed Consent Statement:** Not applicable.

726 **Data Availability Statement:** Not applicable.

727 **Acknowledgments:** We are grateful for the support from the Innovation and Technology Commission of Hong Kong and Undergraduate Research Opportunities Program of the Hong Kong
728 University of Science and Technology.
729

730 **Conflicts of Interest:** The authors declare no conflict of interest.

References

1. Jeong, I.; Finkelstein, J. Introducing Contactless Blood Pressure Assessment Using a High Speed Video Camera. *Journal of Medical Systems* **2016**, *40*, 1–10.
2. Bal, U. Non-contact estimation of heart rate and oxygen saturation using ambient light. *Biomed Opt Express* **2015**, *6*, 86–97.
3. Massaroni, C.; Nicolò, A.; Sacchetti, M.; Schena, E. Contactless Methods For Measuring Respiratory Rate: A Review. *IEEE Sensors Journal* **2021**, *21*, 12821–12839. doi:10.1109/JSEN.2020.3023486.
4. Iozzia, L.; Cerina, L.; Mainardi, L. Relationships between heart-rate variability and pulse-rate variability obtained from video-PPG signal using ZCA. *Physiol Meas* **2016**, *37*, 1934–1944.
5. Scalise, L. Non contact heart monitoring. *Advances in Electrocardiograms-Methods and Analysis* **2012**, *4*, 81–106.
6. Shao, D.; Liu, C.; Tsow, F. Noncontact Physiological Measurement Using a Camera: A Technical Review and Future Directions. *ACS Sensors* **2021**, *6*, 321–334, [<https://doi.org/10.1021/acssensors.0c02042>]. PMID: 33434004, doi:10.1021/acssensors.0c02042.
7. Sun, Y.; Thakor, N. Photoplethysmography Revisited: From Contact to Noncontact, From Point to Imaging. *IEEE Transactions on Biomedical Engineering* **2016**, *63*, 463–477. doi:10.1109/TBME.2015.2476337.
8. Swinehart, D.F. The Beer-Lambert Law. *Journal of Chemical Education* **1962**, *39*, 333, [<https://doi.org/10.1021/ed039p333>]. doi:10.1021/ed039p333.
9. Aarts, L.; Jeanne, V.; Cleary, J.P.; Lieber, C.; Nelson, J.; Bambang-Oetomo, S.; Verkruysse, W. Non-contact heart rate monitoring utilizing camera photoplethysmography in the neonatal intensive care unit — A pilot study. *Early human development* **2013**, *89*. doi:10.1016/j.earlhumdev.2013.09.016.
10. Rouast, P.; Adam, M.; Chiong, R.; Cornforth, D.; Lux, E. Remote heart rate measurement using low-cost RGB face video: A technical literature review. *Frontiers of Computer Science (electronic)* **2018**, *12*, 858–872. doi:10.1007/s11704-016-6243-6.
11. Maurya, L.; Kaur, P.; Chawla, D.; Mahapatra, P. Non-contact breathing rate monitoring in newborns: A review. *Computers in Biology and Medicine* **2021**, *132*, 104321. doi:<https://doi.org/10.1016/j.compbimed.2021.104321>.
12. McDuff, D.J.; Estep, J.R.; Piasecki, A.M.; Blackford, E.B. A survey of remote optical photoplethysmographic imaging methods. 2015 37th Annual International Conference of the IEEE Engineering in Medicine and Biology Society (EMBC), 2015, pp. 6398–6404. doi:10.1109/EMBC.2015.7319857.
13. Wang, W.; den Brinker, A.C.; Stuijk, S.; de Haan, G. Algorithmic Principles of Remote PPG. *IEEE Transactions on Biomedical Engineering* **2017**, *64*, 1479–1491. doi:10.1109/TBME.2016.2609282.
14. Khanam, F.T.Z.; Al-Naji, A.; Chahl, J. Remote Monitoring of Vital Signs in Diverse Non-Clinical and Clinical Scenarios Using Computer Vision Systems: A Review. *Applied Sciences* **2019**, *9*. doi:10.3390/app9204474.
15. Verkruysse, W.; Svaasand, L.O.; Nelson, J.S. Remote plethysmographic imaging using ambient light. *Opt Express* **2008**, *16*, 21434–21445.
16. Poh, M.Z.; McDuff, D.J.; Picard, R.W. Non-contact, automated cardiac pulse measurements using video imaging and blind source separation. *Opt. Express* **2010**, *18*, 10762–10774. doi:10.1364/OE.18.010762.
17. Lewandowska, M.; Rumiński, J.; Kocejko, T.; Nowak, J. Measuring pulse rate with a webcam — A non-contact method for evaluating cardiac activity. 2011 Federated Conference on Computer Science and Information Systems (FedCSIS), 2011, pp. 405–410.
18. de Haan, G.; Jeanne, V. Robust Pulse Rate From Chrominance-Based rPPG. *IEEE Transactions on Biomedical Engineering* **2013**, *60*, 2878–2886. doi:10.1109/TBME.2013.2266196.
19. Tominaga, S. Dichromatic reflection models for a variety of materials. *Color Research & Application* **1994**, *19*, 277 – 285. doi:10.1002/col.5080190408.
20. de Haan, G.; van Leest, A. Improved motion robustness of remote-PPG by using the blood volume pulse signature. *Physiol Meas* **2014**, *35*, 1913–1926.
21. Wang, W.; Stuijk, S.; de Haan, G. A Novel Algorithm for Remote Photoplethysmography: Spatial Subspace Rotation. *IEEE Transactions on Biomedical Engineering* **2016**, *63*, 1974–1984. doi:10.1109/TBME.2015.2508602.
22. Dasari, A.; Arul Prakash, S.K.; Jeni, L.; Tucker, C. Evaluation of biases in remote photoplethysmography methods. *npj Digital Medicine* **2021**, *4*. doi:10.1038/s41746-021-00462-z.
23. Chen, X.; Cheng, J.; Song, R.; Liu, Y.; Ward, R.; Wang, Z.J. Video-Based Heart Rate Measurement: Recent Advances and Future Prospects. *IEEE Transactions on Instrumentation and Measurement* **2019**, *68*, 3600–3615. doi:10.1109/TIM.2018.2879706.
24. Viola, P.; Jones, M. Rapid object detection using a boosted cascade of simple features. Proceedings of the 2001 IEEE Computer Society Conference on Computer Vision and Pattern Recognition. CVPR 2001, 2001, Vol. 1, pp. I–I. doi:10.1109/CVPR.2001.990517.

25. Zhan, Q.; Wang, W.; de Haan, G. Analysis of CNN-based remote-PPG to understand limitations and sensitivities. *Biomedical optics express* **2020**, *11*, 1268–1283.
26. Spetlik, R.; Franc, V.; Cech, J.; Matas, J. Visual Heart Rate Estimation with Convolutional Neural Network. *BMVC*, 2018.
27. Chen, W.; McDuff, D. DeepPhys: Video-Based Physiological Measurement Using Convolutional Attention Networks. *Proceedings of the European Conference on Computer Vision (ECCV)*, 2018.
28. Liu, X.; Fromm, J.; Patel, S.; McDuff, D. Multi-Task Temporal Shift Attention Networks for On-Device Contactless Vitals Measurement. *Neural Information Processing Systems (NeurIPS)*, 2020.
29. Lin, J.; Gan, C.; Han, S. TSM: Temporal Shift Module for Efficient Video Understanding. *Proceedings of the IEEE International Conference on Computer Vision*, 2019.
30. Yu, Z.; Li, X.; Zhao, G. Remote Photoplethysmograph Signal Measurement from Facial Videos Using Spatio-Temporal Networks. *BMVC*, 2019.
31. Yu, Z.; Peng, W.; Li, X.; Hong, X.; Zhao, G. Remote Heart Rate Measurement From Highly Compressed Facial Videos: An End-to-End Deep Learning Solution With Video Enhancement. *2019 IEEE/CVF International Conference on Computer Vision (ICCV)*, 2019, pp. 151–160. doi:10.1109/ICCV.2019.00024.
32. Yu, Z.; Li, X.; Niu, X.; Shi, J.; Zhao, G. AutoHR: A Strong End-to-End Baseline for Remote Heart Rate Measurement With Neural Searching. *IEEE Signal Processing Letters* **2020**, *27*, 1245–1249. doi:10.1109/LSP.2020.3007086.
33. Liu, H.; Simonyan, K.; Yang, Y. DARTS: Differentiable Architecture Search. *International Conference on Learning Representations*, 2019.
34. Xu, Y.; Xie, L.; Zhang, X.; Chen, X.; Qi, G.J.; Tian, Q.; Xiong, H. PC-DARTS: Partial Channel Connections for Memory-Efficient Architecture Search. *International Conference on Learning Representations*, 2019.
35. Hu, M.; Qian, F.; Wang, X.; He, L.; Guo, D.; Ren, F. Robust Heart Rate Estimation with Spatial-Temporal Attention Network from Facial Videos. *IEEE Transactions on Cognitive and Developmental Systems* **2021**, pp. 1–1. doi:10.1109/TCDS.2021.3062370.
36. Qiu, Z.; Yao, T.; Mei, T. Learning Spatio-Temporal Representation with Pseudo-3D Residual Networks. *2017 IEEE International Conference on Computer Vision (ICCV)*, 2017, pp. 5534–5542. doi:10.1109/ICCV.2017.590.
37. Zhang, P.; Li, B.; Peng, J.; Jiang, W. Multi-hierarchical Convolutional Network for Efficient Remote Photoplethysmograph Signal and Heart Rate Estimation from Face Video Clips, 2021, [arXiv:cs.CV/2104.02260].
38. Hu, M.; Qian, F.; Guo, D.; Wang, X.; He, L.; Ren, F. ETA-rPPGNet: Effective Time-Domain Attention Network for Remote Heart Rate Measurement. *IEEE Transactions on Instrumentation and Measurement* **2021**, *70*, 1–12. doi:10.1109/TIM.2021.3058983.
39. Shi, X.; Chen, Z.; Wang, H.; Yeung, D.Y.; Wong, W.k.; Woo, W.c. Convolutional LSTM Network: A Machine Learning Approach for Precipitation Nowcasting. *Proceedings of the 28th International Conference on Neural Information Processing Systems - Volume 1*; MIT Press: Cambridge, MA, USA, 2015; NIPS'15, p. 802–810.
40. Li, X.; Alikhani, I.; Shi, J.; Seppanen, T.; Junttila, J.; Majamaa-Voltti, K.; Tulppo, M.; Zhao, G. The OBF Database: A Large Face Video Database for Remote Physiological Signal Measurement and Atrial Fibrillation Detection. *2018 13th IEEE International Conference on Automatic Face Gesture Recognition (FG 2018)*, 2018, pp. 242–249. doi:10.1109/FG.2018.00043.
41. Hu, M.; Guo, D.; Wang, X.; Ge, P.; Chu, Q. A Novel Spatial-Temporal Convolutional Neural Network for Remote Photoplethysmography. *2019 12th International Congress on Image and Signal Processing, BioMedical Engineering and Informatics (CISP-BMEI)*, 2019, pp. 1–6. doi:10.1109/CISP-BMEI48845.2019.8966034.
42. Lempe, G.; Zaunseder, S.; Wirthgen, T.; Zipser, S.; Malberg, H. ROI Selection for Remote Photoplethysmography. *Bildverarbeitung für die Medizin 2013*; Meinzer, H.P.; Deserno, T.M.; Handels, H.; Tolxdorff, T., Eds.; Springer Berlin Heidelberg: Berlin, Heidelberg, 2013; pp. 99–103.
43. Tang, C.; Lu, J.; Liu, J. Non-contact Heart Rate Monitoring by Combining Convolutional Neural Network Skin Detection and Remote Photoplethysmography via a Low-Cost Camera. *2018 IEEE/CVF Conference on Computer Vision and Pattern Recognition Workshops (CVPRW)*, 2018, pp. 1390–13906. doi:10.1109/CVPRW.2018.00178.
44. Paracchini, M.; Marcon, M.; Villa, F.; Zappa, F.; Tubaro, S. Biometric Signals Estimation Using Single Photon Camera and Deep Learning. *Sensors* **2020**, *20*. doi:10.3390/s20216102.
45. Sabokrou, M.; Pourreza, M.; Li, X.; Fathy, M.; Zhao, G. Deep-HR: Fast Heart Rate Estimation from Face Video Under Realistic Conditions, 2020, [arXiv:cs.CV/2002.04821].
46. Liu, S.; Huang, D.; Wang, Y. Receptive Field Block Net for Accurate and Fast Object Detection. *Computer Vision – ECCV 2018*; Ferrari, V.; Hebert, M.; Sminchisescu, C.; Weiss, Y., Eds.; Springer International Publishing: Cham, 2018; pp. 404–419.
47. Bian, M.; Peng, B.; Wang, W.; Dong, J. An Accurate LSTM Based Video Heart Rate Estimation Method. *Pattern Recognition and Computer Vision*; Lin, Z.; Wang, L.; Yang, J.; Shi, G.; Tan, T.; Zheng, N.; Chen, X.; Zhang, Y., Eds.; Springer International Publishing: Cham, 2019; pp. 409–417.
48. Botina-Monsalve, D.; Benezeth, Y.; Macwan, R.; Pierrart, P.; Parra, F.; Nakamura, K.; Gomez, R.; Miteran, J. Long Short-Term Memory Deep-Filter in Remote Photoplethysmography. *2020 IEEE/CVF Conference on Computer Vision and Pattern Recognition Workshops (CVPRW)*, 2020, pp. 1242–1249. doi:10.1109/CVPRW50498.2020.00161.
49. Liu, X.; Jiang, Z.; Fromm, J.; Xu, X.; Patel, S.; McDuff, D. MetaPhys: Few-Shot Adaptation for Non-Contact Physiological Measurement. In *Proceedings of the Conference on Health, Inference, and Learning*; Association for Computing Machinery: New York, NY, USA, 2021; p. 154–163.

50. Finn, C.; Abbeel, P.; Levine, S. Model-Agnostic Meta-Learning for Fast Adaptation of Deep Networks. *Proceedings of the 34th International Conference on Machine Learning - Volume 70*. JMLR.org, 2017, ICML'17, p. 1126–1135.
51. Bousefsaf, F.; Pruski, A.; Maaoui, C. 3D Convolutional Neural Networks for Remote Pulse Rate Measurement and Mapping from Facial Video. *Applied Sciences* **2019**, *9*. doi:10.3390/app9204364.
52. Tsou, Y.Y.; Lee, Y.A.; Hsu, C.T.; Chang, S.H. Siamese-RPPG Network: Remote Photoplethysmography Signal Estimation from Face Videos. *Proceedings of the 35th Annual ACM Symposium on Applied Computing; Association for Computing Machinery: New York, NY, USA, 2020; SAC '20*, p. 2066–2073. doi:10.1145/3341105.3373905.
53. Perepelkina, O.; Artemyev, M.; Churikova, M.; Grinenko, M. HeartTrack: Convolutional neural network for remote video-based heart rate monitoring. *2020 IEEE/CVF Conference on Computer Vision and Pattern Recognition Workshops (CVPRW)*, 2020, pp. 1163–1171. doi:10.1109/CVPRW50498.2020.00152.
54. Tsou, Y.Y.; Lee, Y.A.; Hsu, C.T. Multi-task Learning for Simultaneous Video Generation and Remote Photoplethysmography Estimation. *Computer Vision – ACCV 2020; Ishikawa, H.; Liu, C.L.; Pajdla, T.; Shi, J., Eds.; Springer International Publishing: Cham, 2021; pp. 392–407*.
55. Liu, S.Q.; Yuen, P.C. A General Remote Photoplethysmography Estimator with Spatiotemporal Convolutional Network. *2020 15th IEEE International Conference on Automatic Face and Gesture Recognition (FG 2020)*, 2020, pp. 481–488. doi:10.1109/FG47880.2020.00109.
56. Wang, Z.K.; Kao, Y.; Hsu, C.T. Vision-Based Heart Rate Estimation Via A Two-Stream CNN. *2019 IEEE International Conference on Image Processing (ICIP)*, 2019, pp. 3327–3331. doi:10.1109/ICIP.2019.8803649.
57. Huang, B.; Chang, C.M.; Lin, C.L.; Chen, W.; Juang, C.F.; Wu, X. Visual Heart Rate Estimation from Facial Video Based on CNN. *2020 15th IEEE Conference on Industrial Electronics and Applications (ICIEA)*, 2020, pp. 1658–1662. doi:10.1109/ICIEA48937.2020.9248356.
58. Lee, E.; Chen, E.; Lee, C.Y. Meta-rPPG: Remote Heart Rate Estimation Using a Transductive Meta-learner. *Computer Vision – ECCV 2020; Vedaldi, A.; Bischof, H.; Brox, T.; Frahm, J.M., Eds.; Springer International Publishing: Cham, 2020; pp. 392–409*.
59. Newell, A.; Yang, K.; Deng, J. Stacked Hourglass Networks for Human Pose Estimation. *Computer Vision – ECCV 2016; Leibe, B.; Matas, J.; Sebe, N.; Welling, M., Eds.; Springer International Publishing: Cham, 2016; pp. 483–499*.
60. Hu, S.X.; Moreno, P.G.; Xiao, Y.; Shen, X.; Obozinski, G.; Lawrence, N.; Damianou, A. Empirical Bayes Transductive Meta-Learning with Synthetic Gradients. *International Conference on Learning Representations*, 2020.
61. Huang, B.; Lin, C.L.; Chen, W.; Juang, C.F.; Wu, X. A novel one-stage framework for visual pulse rate estimation using deep neural networks. *Biomedical Signal Processing and Control* **2021**, *66*, 102387. doi:https://doi.org/10.1016/j.bspc.2020.102387.
62. Song, R.; Chen, H.; Cheng, J.; Li, C.; Liu, Y.; Chen, X. PulseGAN: Learning to Generate Realistic Pulse Waveforms in Remote Photoplethysmography. *IEEE Journal of Biomedical and Health Informatics* **2021**, *25*, 1373–1384. doi:10.1109/JBHI.2021.3051176.
63. Mirza, M.; Osindero, S. Conditional Generative Adversarial Nets, 2014, [arXiv:cs.LG/1411.1784].
64. Yang, W.; Li, X.; Zhang, B. Heart Rate Estimation from Facial Videos Based on Convolutional Neural Network. *2018 International Conference on Network Infrastructure and Digital Content (IC-NIDC)*, 2018, pp. 45–49. doi:10.1109/ICNIDC.2018.8525602.
65. He, K.; Zhang, X.; Ren, S.; Sun, J. Deep Residual Learning for Image Recognition. *2016 IEEE Conference on Computer Vision and Pattern Recognition (CVPR)*, 2016, pp. 770–778. doi:10.1109/CVPR.2016.90.
66. Niu, X.; Han, H.; Shan, S.; Chen, X. SynRhythm: Learning a Deep Heart Rate Estimator from General to Specific. *2018 24th International Conference on Pattern Recognition (ICPR)*, 2018, pp. 3580–3585. doi:10.1109/ICPR.2018.8546321.
67. Niu, X.; Shan, S.; Han, H.; Chen, X. RhythmNet: End-to-End Heart Rate Estimation From Face via Spatial-Temporal Representation. *IEEE Transactions on Image Processing* **2020**, *29*, 2409–2423. doi:10.1109/TIP.2019.2947204.
68. Niu, X.; Yu, Z.; Han, H.; Li, X.; Shan, S.; Zhao, G. Video-based remote physiological measurement via cross-verified feature disentangling. *European Conference on Computer Vision*. Springer, 2020, pp. 295–310.
69. Song, R.; Zhang, S.; Li, C.; Zhang, Y.; Cheng, J.; Chen, X. Heart Rate Estimation From Facial Videos Using a Spatiotemporal Representation With Convolutional Neural Networks. *IEEE Transactions on Instrumentation and Measurement* **2020**, *69*, 7411–7421. doi:10.1109/TIM.2020.2984168.
70. Lu, H.; Han, H. NAS-HR: Neural architecture search for heart rate estimation from face videos. *Virtual Reality & Intelligent Hardware* **2021**, *3*, 33–42. doi:https://doi.org/10.1016/j.vrih.2020.10.002.
71. Niu, X.; Zhao, X.; Han, H.; Das, A.; Dantcheva, A.; Shan, S.; Chen, X. Robust Remote Heart Rate Estimation from Face Utilizing Spatial-temporal Attention. *2019 14th IEEE International Conference on Automatic Face Gesture Recognition (FG 2019)*, 2019, pp. 1–8. doi:10.1109/FG.2019.8756554.
72. Meziatisabour, R.; Benezeth, Y.; De Oliveira, P.; Chappe, J.; Yang, F. UBFC-Phys: A Multimodal Database For Psychophysiological Studies Of Social Stress. *IEEE Transactions on Affective Computing* **2021**, pp. 1–1. doi:10.1109/TAFFC.2021.3056960.
73. McDuff, D.; Gontarek, S.; Picard, R. Remote measurement of cognitive stress via heart rate variability. *2014 36th Annual International Conference of the IEEE Engineering in Medicine and Biology Society*, 2014, pp. 2957–2960. doi:10.1109/EMBC.2014.6944243.
74. Gupta, P.; Bhowmick, B.; Pal, A. Exploring the Feasibility of Face Video Based Instantaneous Heart-Rate for Micro-Expression Spotting. *2018 IEEE/CVF Conference on Computer Vision and Pattern Recognition Workshops (CVPRW)*, 2018, pp. 1397–13977. doi:10.1109/CVPRW.2018.00179.
75. Monkaresi, H.; Bosch, N.; Calvo, R.A.; D’Mello, S.K. Automated Detection of Engagement Using Video-Based Estimation of Facial Expressions and Heart Rate. *IEEE Transactions on Affective Computing* **2017**, *8*, 15–28. doi:10.1109/TAFFC.2016.2515084.

76. Kessler, V.; Thiam, P.; Amirian, M.; Schwenker, F. Pain recognition with camera photoplethysmography. 2017 Seventh International Conference on Image Processing Theory, Tools and Applications (IPTA), 2017, pp. 1–5. doi:10.1109/IPTA.2017.8310110.
77. Huang, D.; Feng, X.; Zhang, H.; Yu, Z.; Peng, J.; Zhao, G.; Xia, Z. Spatio-Temporal Pain Estimation Network with Measuring Pseudo Heart Rate Gain. *IEEE Transactions on Multimedia* **2021**, pp. 1–1. doi:10.1109/TMM.2021.3096080.
78. Yang, R.; Guan, Z.; Yu, Z.; Zhao, G.; Feng, X.; Peng, J. Non-contact Pain Recognition from Video Sequences with Remote Physiological Measurements Prediction. *arXiv preprint arXiv:2105.08822* **2021**.
79. Mitra, B.; Luckhoff, C.; Mitchell, R.D.; O'Reilly, G.M.; Smit, D.V.; Cameron, P.A. Temperature screening has negligible value for control of COVID-19. *Emergency Medicine Australasia* **2020**, *32*, 867–869, [<https://onlinelibrary.wiley.com/doi/pdf/10.1111/1742-6723.13578>]. doi:<https://doi.org/10.1111/1742-6723.13578>.
80. Vilke, G.M.; Brennan, J.J.; Cronin, A.O.; Castillo, E.M. Clinical Features of Patients with COVID-19: is Temperature Screening Useful? *The Journal of Emergency Medicine* **2020**, *59*, 952–956. doi:<https://doi.org/10.1016/j.jemermed.2020.09.048>.
81. Stave, G.M.; Smith, S.E.; Hymel, P.A.; Heron, R.J.L. Worksite Temperature Screening for COVID-19. *J Occup Environ Med* **2021**.
82. Lippi, G.; Mattiuzzi, C.; Henry, B. Is Body Temperature Mass Screening a Reliable and Safe Option for Preventing COVID-19 Spread? *SSRN Electronic Journal* **2021**. doi:10.2139/ssrn.3779727.
83. Natarajan, A.; Su, H.W.; Heneghan, C. Assessment of physiological signs associated with COVID-19 measured using wearable devices. *medRxiv* **2020**, [<https://www.medrxiv.org/content/early/2020/08/16/2020.08.14.20175265.full.pdf>]. doi:10.1101/2020.08.14.20175265.
84. Pavri, B.; Kloof, J.; Farzad, D.; Riley, J. Behavior of the PR Interval with Increasing Heart Rate in Patients with COVID-19. *Heart Rhythm* **2020**, *17*. doi:10.1016/j.hrthm.2020.06.009.
85. Gawalko, M.; Kapłan-Cieślicka, A.; Hohl, M.; Dobrev, D.; Linz, D. COVID-19 associated atrial fibrillation: Incidence, putative mechanisms and potential clinical implications. *International journal of cardiology. Heart & vasculature* **2020**, *30*.
86. Stone, E.; Kiat, H.; McLachlan, C.S. Atrial fibrillation in COVID-19: A review of possible mechanisms. *The FASEB Journal* **2020**, *34*, 11347–11354.
87. Schnaubelt, S.; Breyer, M.K.; Siller-Matula, J.; Domanovits, H. Atrial fibrillation: a risk factor for unfavourable outcome in COVID-19? A case report. *European Heart Journal-Case Reports* **2020**.
88. Shi, J.; Alikhani, I.; Li, X.; Yu, Z.; Seppänen, T.; Zhao, G. Atrial Fibrillation Detection From Face Videos by Fusing Subtle Variations. *IEEE Transactions on Circuits and Systems for Video Technology* **2020**, *30*, 2781–2795. doi:10.1109/TCSVT.2019.2926632.
89. Zhu, G.; Li, J.; Meng, Z.; Yu, Y.; Li, Y.; Tang, X.; Dong, Y.; Sun, G.; Zhou, R.; Wang, H.; Wang, K.; Huang, W. Learning from Large-Scale Wearable Device Data for Predicting the Epidemic Trend of COVID-19. *Discrete Dynamics in Nature and Society* **2020**, *2020*, 1–8. doi:10.1155/2020/6152041.
90. Mishra, T.; Wang, M.; Metwally, A.A.; Bogu, G.K.; Brooks, A.W.; Bahmani, A.; Alavi, A.; Celli, A.; Higgs, E.; Dagan-Rosenfeld, O.; Fay, B.; Kirkpatrick, S.; Kellogg, R.; Gibson, M.; Wang, T.; Hunting, E.M.; Mamic, P.; Ganz, A.B.; Rolnik, B.; Li, X.; Snyder, M.P. Pre-symptomatic detection of COVID-19 from smartwatch data. *Nat Biomed Eng* **2020**, *4*, 1208–1220.
91. Suwajanakorn, S.; Seitz, S.M.; Kemelmacher-Shlizerman, I. Synthesizing Obama: Learning Lip Sync from Audio. *ACM Trans. Graph.* **2017**, *36*. doi:10.1145/3072959.3073640.
92. Nguyen, T.; Nguyen, C.; Nguyen, D.; Nguyen, D.; Nahavandi, S. Deep Learning for Deepfakes Creation and Detection. *ArXiv* **2019**, *abs/1909.11573*.
93. Korshunov, P.; Marcel, S. DeepFakes: a New Threat to Face Recognition? Assessment and Detection. *ArXiv* **2018**, *abs/1812.08685*.
94. Westerlund, M. The Emergence of Deepfake Technology: A Review. *Technology Innovation Management Review* **2019**, *9*, 40–53. doi:<http://doi.org/10.22215/timreview/1282>.
95. Fernandes, S.; Raj, S.; Ortiz, E.; Vintila, I.; Salter, M.; Urosevic, G.; Jha, S. Predicting Heart Rate Variations of Deepfake Videos using Neural ODE. 2019 IEEE/CVF International Conference on Computer Vision Workshop (ICCVW), 2019, pp. 1721–1729. doi:10.1109/ICCVW.2019.00213.
96. Ciftci, U.; Demir, I.; Yin, L. FakeCatcher: Detection of Synthetic Portrait Videos using Biological Signals. *IEEE Transactions on Pattern Analysis and Machine Intelligence* **2020**, *PP*, 1–1. doi:10.1109/TPAMI.2020.3009287.
97. Tuckson, R.V.; Edmunds, M.; Hodgkins, M.L. Telehealth. *New England Journal of Medicine* **2017**, *377*, 1585–1592, [<https://doi.org/10.1056/NEJMs1503323>]. PMID: 29045204, doi:10.1056/NEJMs1503323.
98. Song, R.; Li, J.; Wang, M.; Cheng, J.; Li, C.; Chen, X. Remote Photoplethysmography With an EEMD-MCCA Method Robust Against Spatially Uneven Illuminations. *IEEE Sensors Journal* **2021**, *21*, 13484–13494. doi:10.1109/JSEN.2021.3067770.
99. Zhao, F.; Li, M.; Qian, Y.; Tsien, J.Z. Remote Measurements of Heart and Respiration Rates for Telemedicine. *PLOS ONE* **2013**, *8*, 1–14. doi:10.1371/journal.pone.0071384.
100. Zhou, X.; Snoswell, C.L.; Harding, L.E.; Bambling, M.; Edirippulige, S.; Bai, X.; Smith, A.C. The Role of Telehealth in Reducing the Mental Health Burden from COVID-19. *Telemedicine and e-Health* **2020**, *26*, 377–379, [<https://doi.org/10.1089/tmj.2020.0068>]. PMID: 32202977, doi:10.1089/tmj.2020.0068.
101. Alsaadi, I. Physiological Biometric Authentication Systems, Advantages, Disadvantages And Future Development: A Review. *International Journal of Scientific & Technology Research* **2015**, *Volume 4*.
102. Kumar, S.; Singh, S.; Kumar, J. A comparative study on face spoofing attacks. 2017 International Conference on Computing, Communication and Automation (ICCCA), 2017, pp. 1104–1108. doi:10.1109/CCAA.2017.8229961.

103. Yu, Z.; Qin, Y.; Li, X.; Zhao, C.; Lei, Z.; Zhao, G. Deep learning for face anti-spoofing: a survey. *arXiv preprint arXiv:2106.14948* **2021**.
104. Liu, S.Q.; Lan, X.; Yuen, P.C. Remote Photoplethysmography Correspondence Feature for 3D Mask Face Presentation Attack Detection. Proceedings of the European Conference on Computer Vision (ECCV), 2018.
105. Li, X.; Komulainen, J.; Zhao, G.; Yuen, P.C.; Pietikäinen, M. Generalized face anti-spoofing by detecting pulse from face videos. 2016 23rd International Conference on Pattern Recognition (ICPR). IEEE, 2016, pp. 4244–4249.
106. Liu, S.; Yuen, P.C.; Zhang, S.; Zhao, G. 3D Mask Face Anti-spoofing with Remote Photoplethysmography. Computer Vision – ECCV 2016; Leibe, B.; Matas, J.; Sebe, N.; Welling, M., Eds.; Springer International Publishing: Cham, 2016; pp. 85–100.
107. Yu, Z.; Li, X.; Wang, P.; Zhao, G. TransRPPG: Remote Photoplethysmography Transformer for 3D Mask Face Presentation Attack Detection. *ArXiv* **2021**, *abs/2104.07419*.
108. Lin, B.; Li, X.; Yu, Z.; Zhao, G. Face liveness detection by rppg features and contextual patch-based cnn. Proceedings of the 2019 3rd International Conference on Biometric Engineering and Applications, 2019, pp. 61–68.
109. Kuo, J.; Koppel, S.; Charlton, J.L.; Rudin-Brown, C.M. Evaluation of a video-based measure of driver heart rate. *Journal of Safety Research* **2015**, *54*, 55.e29–59. Strategic Highway Research Program (SHRP 2) and Special Issue: Fourth International Symposium on Naturalistic Driving Research, doi:<https://doi.org/10.1016/j.jsr.2015.06.009>.
110. Zhang, Q.; Xu, G.q.; Wang, M.; Zhou, Y.; Feng, W. Webcam based non-contact real-time monitoring for the physiological parameters of drivers. The 4th Annual IEEE International Conference on Cyber Technology in Automation, Control and Intelligent, 2014, pp. 648–652. doi:[10.1109/CYBER.2014.6917541](https://doi.org/10.1109/CYBER.2014.6917541).
111. Lee, K.; Han, D.; ko, H. Video Analytic Based Health Monitoring for Driver in Moving Vehicle by Extracting Effective Heart Rate Inducing Features. *Journal of Advanced Transportation* **2018**, *2018*, 1–9. doi:[10.1155/2018/8513487](https://doi.org/10.1155/2018/8513487).
112. Zhang, Q.; Zhou, Y.; Song, S.; Liang, G.; Ni, H. Heart Rate Extraction Based on Near-Infrared Camera: Towards Driver State Monitoring. *IEEE Access* **2018**, *6*, 33076–33087. doi:[10.1109/ACCESS.2018.2845390](https://doi.org/10.1109/ACCESS.2018.2845390).
113. Wu, B.F.; Chu, Y.W.; Huang, P.W.; Chung, M.L. Neural Network Based Luminance Variation Resistant Remote-Photoplethysmography for Driver’s Heart Rate Monitoring. *IEEE Access* **2019**, *7*, 57210–57225. doi:[10.1109/ACCESS.2019.2913664](https://doi.org/10.1109/ACCESS.2019.2913664).
114. Huang, P.W.; Wu, B.J.; Wu, B.F. A Heart Rate Monitoring Framework for Real-World Drivers Using Remote Photoplethysmography. *IEEE Journal of Biomedical and Health Informatics* **2021**, *25*, 1397–1408. doi:[10.1109/JBHI.2020.3026481](https://doi.org/10.1109/JBHI.2020.3026481).
115. Tsai, Y.C.; Lai, P.W.; Huang, P.W.; Lin, T.M.; Wu, B.F. Vision-Based Instant Measurement System for Driver Fatigue Monitoring. *IEEE Access* **2020**, *8*, 67342–67353. doi:[10.1109/ACCESS.2020.2986234](https://doi.org/10.1109/ACCESS.2020.2986234).
116. Magdalena Nowara, E.; Marks, T.K.; Mansour, H.; Veeraraghavan, A. SparsePPG: Towards Driver Monitoring Using Camera-Based Vital Signs Estimation in Near-Infrared. Proceedings of the IEEE Conference on Computer Vision and Pattern Recognition (CVPR) Workshops, 2018.
117. Wu, B.F.; Chu, Y.W.; Huang, P.W.; Chung, M.L.; Lin, T.M. A Motion Robust Remote-PPG Approach to Driver’s Health State Monitoring. Computer Vision – ACCV 2016 Workshops; Chen, C.S.; Lu, J.; Ma, K.K., Eds.; Springer International Publishing: Cham, 2017; pp. 463–476.
118. Hernandez-Ortega, J.; Nagae, S.; Fierrez, J.; Morales, A. Quality-Based Pulse Estimation from NIR Face Video with Application to Driver Monitoring. Pattern Recognition and Image Analysis; Morales, A.; Fierrez, J.; Sánchez, J.S.; Ribeiro, B., Eds.; Springer International Publishing: Cham, 2019; pp. 108–119.
119. Al-Naji, A.A.; Perera, A.; Chahl, J. Remote measurement of cardiopulmonary signal using an unmanned aerial vehicle. IOP Conference Series: Materials Science and Engineering, 2018, Vol. 405, p. 012001. doi:[10.1088/1757-899X/405/1/012001](https://doi.org/10.1088/1757-899X/405/1/012001).
120. Al-Naji, A.A.; Perera, A.; Chahl, J. Remote monitoring of cardiorespiratory signals from a hovering unmanned aerial vehicle. *BioMedical Engineering OnLine* **2017**, *16*. doi:[10.1186/s12938-017-0395-y](https://doi.org/10.1186/s12938-017-0395-y).
121. Al-Naji, A.; Perera, A.G.; Mohammed, S.L.; Chahl, J. Life Signs Detector Using a Drone in Disaster Zones. *Remote Sensing* **2019**, *11*. doi:[10.3390/rs11202441](https://doi.org/10.3390/rs11202441).
122. Al-Naji, A.; Chahl, J. Remote Optical Cardiopulmonary Signal Extraction With Noise Artifact Removal, Multiple Subject Detection Long-Distance. *IEEE Access* **2018**, *6*, 11573–11595. doi:[10.1109/ACCESS.2018.2811392](https://doi.org/10.1109/ACCESS.2018.2811392).
123. Klaessens, J.H.; van den Born, M.; van der Veen, A.; van de Kraats, J.S.; van den Dungen, F.A.; Verdaasdonk, R.M. Development of a baby friendly non-contact method for measuring vital signs: First results of clinical measurements in an open incubator at a neonatal intensive care unit. Advanced Biomedical and Clinical Diagnostic Systems XII; Vo-Dinh, T.; Mahadevan-Jansen, A.; M.D., W.S.G., Eds. International Society for Optics and Photonics, SPIE, 2014, Vol. 8935, pp. 257 – 263.
124. Villarroel, M.; Guazzi, A.; Jorge, J.; Davis, S.; Watkinson, P.; Green, G.; Shenvi, A.; McCormick, K.; Tarassenko, L. Continuous non-contact vital sign monitoring in neonatal intensive care unit. *Healthcare Technology Letters* **2014**, *1*, 87–91(4).
125. Aarts, L.A.; Jeanne, V.; Cleary, J.P.; Lieber, C.; Nelson, J.S.; Bambang Oetomo, S.; Verkruysse, W. Non-contact heart rate monitoring utilizing camera photoplethysmography in the neonatal intensive care unit - a pilot study. *Early Hum Dev* **2013**, *89*, 943–948.
126. Scalise, L.; Bernacchia, N.; Ercoli, I.; Marchionni, P. Heart rate measurement in neonatal patients using a webcam. 2012 IEEE International Symposium on Medical Measurements and Applications Proceedings, 2012, pp. 1–4. doi:[10.1109/MeMeA.2012.6226654](https://doi.org/10.1109/MeMeA.2012.6226654).
127. Cobos-Torres, J.C.; Abderrahim, M.; Martínez-Orgado, J. Non-Contact, Simple Neonatal Monitoring by Photoplethysmography. *Sensors* **2018**, *18*. doi:[10.3390/s18124362](https://doi.org/10.3390/s18124362).

128. Gibson, K.; Al-Najji, A.; Fleet, J.A.; Steen, M.; Chahl, J.; Huynh, J.; Morris, S. Noncontact Heart and Respiratory Rate Monitoring of Preterm Infants Based on a Computer Vision System: Protocol for a Method Comparison Study. *JMIR Res Protoc* **2019**, *8*, e13400. doi:10.2196/13400.
129. Mestha, L.K.; Kyal, S.; Xu, B.; Lewis, L.E.; Kumar, V. Towards continuous monitoring of pulse rate in neonatal intensive care unit with a webcam. 2014 36th Annual International Conference of the IEEE Engineering in Medicine and Biology Society, 2014, pp. 3817–3820. doi:10.1109/EMBC.2014.6944455.
130. van Gastel, M.; Balmaekers, B.; Oetomo, S.B.; Verkruysse, W. Near-continuous non-contact cardiac pulse monitoring in a neonatal intensive care unit in near darkness. *Optical Diagnostics and Sensing XVIII: Toward Point-of-Care Diagnostics*; Coté, G.L., Ed. International Society for Optics and Photonics, SPIE, 2018, Vol. 10501, pp. 230 – 238.
131. Malafaya, D.; Domingues, S.; Oliveira, H.P. Domain Adaptation for Heart Rate Extraction in the Neonatal Intensive Care Unit. 2020 IEEE International Conference on Bioinformatics and Biomedicine (BIBM), 2020, pp. 1082–1086. doi:10.1109/BIBM49941.2020.9313123.
132. Antink, C.H.; Ferreira, J.C.M.; Paul, M.; Lyra, S.; Heimann, K.; Karthik, S.; Joseph, J.; Jayaraman, K.; Orlikowsky, T.; Sivaprakasam, M.; Leonhardt, S. Fast body part segmentation and tracking of neonatal video data using deep learning. *Med Biol Eng Comput* **2020**, *58*, 3049–3061.
133. Chaichulee, S.; Villarroel, M.; Jorge, J.; Arteta, C.; McCormick, K.; Zisserman, A.; Tarassenko, L. Cardio-respiratory signal extraction from video camera data for continuous non-contact vital sign monitoring using deep learning. *Physiological Measurement* **2019**, *40*, 115001. doi:10.1088/1361-6579/ab525c.
134. Wang, W.; den Brinker, A.C.; Stuijk, S.; de Haan, G. Robust heart rate from fitness videos. *Physiol Meas* **2017**, *38*, 1023–1044.
135. Chang, C.M.; Hung, C.C.; Zhao, C.; Lin, C.L.; Hsu, B.Y. Learning-based Remote Photoplethysmography for Physiological Signal Feedback Control in Fitness Training. 2020 15th IEEE Conference on Industrial Electronics and Applications (ICIEA), 2020, pp. 1663–1668. doi:10.1109/ICIEA48937.2020.9248164.
136. Zhao, C.; Lin, C.L.; Chen, W.; Chen, M.K.; Wang, J. Visual heart rate estimation and negative feedback control for fitness exercise. *Biomedical Signal Processing and Control* **2020**, *56*, 101680. doi:https://doi.org/10.1016/j.bspc.2019.101680.
137. de Haan, G.; van Leest, A. Improved motion robustness of remote-PPG by using the blood volume pulse signature. *Physiological Measurement* **2014**, *35*, 1913–1926. doi:10.1088/0967-3334/35/9/1913.
138. Xie, K.; Fu, C.H.; Liang, H.; Hong, H.; Zhu, X. Non-contact Heart Rate Monitoring for Intensive Exercise Based on Singular Spectrum Analysis. 2019 IEEE Conference on Multimedia Information Processing and Retrieval (MIPR), 2019, pp. 228–233. doi:10.1109/MIPR.2019.00048.
139. McDuff, D.; Blackford, E. iPhys: An Open Non-Contact Imaging-Based Physiological Measurement Toolbox. 2019 41st Annual International Conference of the IEEE Engineering in Medicine and Biology Society (EMBC), 2019, pp. 6521–6524. doi:10.1109/EMBC.2019.8857012.
140. van der Kooij, K.M.; Naber, M. An open-source remote heart rate imaging method with practical apparatus and algorithms. *Behav Res Methods* **2019**, *51*, 2106–2119.
141. Boccignone, G.; Conte, D.; Cuculo, V.; D’Amelio, A.; Grossi, G.; Lanzarotti, R. An Open Framework for Remote-PPG Methods and Their Assessment. *IEEE Access* **2020**, *8*, 216083–216103. doi:10.1109/ACCESS.2020.3040936.
142. Estep, J.R.; Blackford, E.B.; Meier, C.M. Recovering pulse rate during motion artifact with a multi-imager array for non-contact imaging photoplethysmography. 2014 IEEE International Conference on Systems, Man, and Cybernetics (SMC), 2014, pp. 1462–1469. doi:10.1109/SMC.2014.6974121.
143. Heusch, G.; Anjos, A.; Marcel, S. A Reproducible Study on Remote Heart Rate Measurement. *CoRR* **2017**, *abs/1709.00962*, [1709.00962].
144. Soleymani, M.; Lichtenauer, J.; Pun, T.; Pantic, M. A Multimodal Database for Affect Recognition and Implicit Tagging. *IEEE Transactions on Affective Computing* **2012**, *3*, 42–55. doi:10.1109/T-AFFC.2011.25.
145. Zhang, Z.; Girard, J.M.; Wu, Y.; Zhang, X.; Liu, P.; Ciftci, U.; Canavan, S.; Reale, M.; Horowitz, A.; Yang, H.; Cohn, J.F.; Ji, Q.; Yin, L. Multimodal Spontaneous Emotion Corpus for Human Behavior Analysis. 2016 IEEE Conference on Computer Vision and Pattern Recognition (CVPR), 2016, pp. 3438–3446. doi:10.1109/CVPR.2016.374.
146. Stricker, R.; Müller, S.; Gross, H.M. Non-contact video-based pulse rate measurement on a mobile service robot. The 23rd IEEE International Symposium on Robot and Human Interactive Communication, 2014, pp. 1056–1062. doi:10.1109/ROMAN.2014.6926392.
147. Bobbia, S.; Macwan, R.; Benezeth, Y.; Mansouri, A.; Dubois, J. Unsupervised skin tissue segmentation for remote photoplethysmography. *Pattern Recognition Letters* **2019**, *124*, 82–90. Award Winning Papers from the 23rd International Conference on Pattern Recognition (ICPR), doi:https://doi.org/10.1016/j.patrec.2017.10.017.
148. Niu, X.; Han, H.; Shan, S.; Chen, X. VIPL-HR: A Multi-modal Database for Pulse Estimation from Less-constrained Face Video. *ACCV*, 2018.
149. Russakovsky, O.; Deng, J.; Su, H.; Krause, J.; Satheesh, S.; Ma, S.; Huang, Z.; Karpathy, A.; Khosla, A.; Bernstein, M.; others. Imagenet large scale visual recognition challenge. *International journal of computer vision* **2015**, *115*, 211–252.
150. Li, X.; Han, H.; Lu, H.; Niu, X.; Yu, Z.; Dantcheva, A.; Zhao, G.; Shan, S. The 1st Challenge on Remote Physiological Signal Sensing (RePSS). 2020 IEEE/CVF Conference on Computer Vision and Pattern Recognition Workshops (CVPRW), 2020, pp. 1274–1281. doi:10.1109/CVPRW50498.2020.00165.

151. Nowara, E.M.; McDuff, D.; Veeraraghavan, A. Systematic analysis of video-based pulse measurement from compressed videos. *Biomedical Optics Express* **2021**, *12*, 494–508.
152. Kenzaka, T.; Okayama, M.; Kuroki, S.; Fukui, M.; Yahata, S.; Hayashi, H.; Kitao, A.; Sugiyama, D.; Kajii, E.; Hashimoto, M. Importance of vital signs to the early diagnosis and severity of sepsis: association between vital signs and sequential organ failure assessment score in patients with sepsis. *Intern Med* **2012**, *51*, 871–876.
153. Chalari, E.; Intas, G.; Stergiannis, P.; Vezyridis, P.; Paraskevas, V.; Fildissis, G. The importance of vital signs in the triage of injured patients. *Crit Care Nurs Q* **2012**, *35*, 292–298.
154. Manta, C.; Jain, S.S.; Coravos, A.; Mendelsohn, D.; Izmailova, E.S. An Evaluation of Biometric Monitoring Technologies for Vital Signs in the Era of COVID-19. *Clinical and Translational Science* **2020**, *13*, 1034–1044.
155. Pimentel, M.A.; Redfern, O.C.; Hatch, R.; Young, J.D.; Tarassenko, L.; Watkinson, P.J. Trajectories of vital signs in patients with COVID-19. *Resuscitation* **2020**, *156*, 99–106.
156. Djeldjli, D.; Bousefsaf, F.; Maaoui, C.; Bereksi-Reguig, F.; Pruski, A. Remote estimation of pulse wave features related to arterial stiffness and blood pressure using a camera. *Biomedical Signal Processing and Control* **2021**, *64*, 102242. doi:<https://doi.org/10.1016/j.bspc.2020.102242>.
157. Luo, H.; Yang, D.; Barszczyk, A.; Vempala, N.; Wei, J.; Wu, S.J.; Zheng, P.P.; Fu, G.; Lee, K.; Feng, Z.P. Smartphone-based blood pressure measurement using transdermal optical imaging technology. *Circulation: Cardiovascular Imaging* **2019**, *12*, e008857.
158. Fan, X.; Ye, Q.; Yang, X.; Choudhury, S.D. Robust blood pressure estimation using an RGB camera. *Journal of Ambient Intelligence and Humanized Computing* **2020**, *11*, 4329–4336.
159. Casalino, G.; Castellano, G.; Zaza, G. A mHealth solution for contact-less self-monitoring of blood oxygen saturation. 2020 IEEE Symposium on Computers and Communications (ISCC), 2020, pp. 1–7. doi:10.1109/ISCC50000.2020.9219718.
160. Shao, D.; Liu, C.; Tsow, F.; Yang, Y.; Du, Z.; Iriya, R.; Yu, H.; Tao, N. Noncontact Monitoring of Blood Oxygen Saturation Using Camera and Dual-Wavelength Imaging System. *IEEE Transactions on Biomedical Engineering* **2016**, *63*, 1091–1098. doi:10.1109/TBME.2015.2481896.
161. Kong, L.; Zhao, Y.; Dong, L.; Jian, Y.; Jin, X.; Li, B.; Feng, Y.; Liu, M.; Liu, X.; Wu, H. Non-contact detection of oxygen saturation based on visible light imaging device using ambient light. *Opt. Express* **2013**, *21*, 17464–17471. doi:10.1364/OE.21.017464.
162. Nowara, E.M.; McDuff, D.; Veeraraghavan, A. A meta-analysis of the impact of skin tone and gender on non-contact photoplethysmography measurements. Proceedings of the IEEE/CVF Conference on Computer Vision and Pattern Recognition Workshops, 2020, pp. 284–285.
163. Hassan, M.; Malik, A.; Fofi, D.; Karasfi, B.; Meriaudeau, F. Towards health monitoring using remote heart rate measurement using digital camera: A feasibility study. *Measurement* **2020**, *149*, 106804.
164. Blackford, E.B.; Estep, J.R. Measurements of pulse rate using long-range imaging photoplethysmography and sunlight illumination outdoors. Optical Diagnostics and Sensing XVII: Toward Point-of-Care Diagnostics. International Society for Optics and Photonics, 2017, Vol. 10072, p. 100720S.